Designing a compliant hip-back support for an exoskeleton

T.O.M.E. Cratsborn

Delft University of Technology

TU Delft

Designing a compliant hip-back support for an exoskeleton

by

T.O.M.E. Cratsborn

to obtain the degree of Master of Science
at the Delft University of Technology,
to be defended publicly on Friday February 19, 2021 at 2:30 PM.

Student number:	4374118	
Project duration:	February 10, 2020 – February 19, 2021	
Thesis committee:	Prof. dr. ir. J.L. Herder,	TU Delft, chair
	Dr. J.J. van den Dobbelsteen,	TU Delft
	Dr. ir. G. Radaelli,	TU Delft
	MSc. A. A. Nobaveh,	TU Delft, supervisor

This thesis is confidential and cannot be made public until February 19, 2022.

TU Delft

Preface

"A good teacher must know the rules; a good pupil, the exceptions." - Martin H. Fischer

Now, I have come to the beginning of the end. This preface does not only mark the end of my thesis or my master but the end of 6 and a half years of studying at the university. I learned a lot of new skills, collected a lot of knowledge but most importantly, I got to know a lot of bright and amazing people without whom I would have never gotten this far.

I would like to thank my supervisors Ali and Giuseppe for all the fruitful discussions and great guidance during this project. Furthermore to the shellskeleton research group itself, thank you for all the discussions, and keep up the good work!

I would also like to thank the people from the IWS at 3mE who helped me manufacture my prototypes and the support staff from PME who helped me with the experiments and test setup.

Thanks to my friends and the critical reviewers for the coffee moments and feedback along the way. And last but not least my family and girlfriend whom without, this would not have been possible.

So without any further ado, and with great enthusiasm, I hereby present my thesis project. I hope you enjoy it as much as I did.

T.O.M.E. Cratsborn
Delft, February 2021

Contents

1

Summary

This report is written for the thesis of my master Mechanical Engineering that was conducted at the department Precision and Microsystems Engineering of the Delft University of Technology. The goal of the project was to design a compliant hip-back support of an exoskeleton while researching how to achieve desired directional compliance on this application.

This work starts with an introduction to exoskeletons and explaining their working principles. The problem is that the reduction of range of motion for wearing an exoskeleton reduces the adoption of exoskeletons in industry. The objective of this study was to solve this by creating a hip-back support with compliant behaviour in torsion and lateral bending while remaining stiff in the supporting forward bending direction. For inspiration, the state of the art of current hip-back supports and research projects was reviewed. Also, the characterization methods of compliant mechanisms were reviewed for inspiration, to come up with a suitable design method for developing a compliant structure for a hip-back support. By tuning stiffness of the structure in distinct directions, a conventional synthesis method for compliant mechanisms could be applied, namely the Freedom and Constraint Topologies method. This was used to come up with a preliminary design. This design was extended to improve stiffness behaviour for coupled motions by researching how to change stiffness on demand. The only categories to change stiffness are shape, material, prestress and boundary condition. For each category, a promising high-level design was worked out with improved stiffness behaviour for coupled motions. To generate an even more satisfying solution, optimization of the beam shape was applied to handle the defined rather complex kinetostatic task and to develop a lightweight structure. The objective function was to reach specified deflections where shape-related parameters are optimized. These parameters were the spine shape of the beam, the cross-section and orientation of the cross-section. To generate a design, a self-developed optimizer using beam modelling was extended and applied. The extensions were to optimize a double-clamped beam that was loaded in the middle point and optimizing for angular deformations as a set objective function. This extended optimizer generated the final design which was a thin rectangular-shaped beam with three-dimensional curves. This design was not straightforward to fabricate into a prototype. Multiple manufacturing methods were evaluated and one final method was selected to fabricate a close approximation of the final design. This final manufacturing method was to produce the prototype by roll bending and manually applying a twist on a curved laser-cut strip which was extracted from flattening of the spatial shape. This prototype was verified by simulations and experiments. Simulation tests were run on an original design of the back support and compared with the new optimized shape based on the requirements. The results, for similar loadings and material, are 27 times more lateral flexibility, 1.25 more torsional flexibility and a design that is four times lighter in comparison to the original design. The original relative stiffness of 1 to 1 for forward relative to lateral bending improved to 2 to 1. An important remark to note is that the beam model generated a thin section which was less suitable for 1D beam modelling of the implemented FEM. Creating an optimizer based on 2D shell modelling code might give more accurate results and can be considered for future work.

2

Introduction

Repetitive lifting and carrying of heavy objects are two main reasons for work-related lower back pain (LBP) [1]. LBP is one of the most common occupational diseases in various industries. Particularly high prevalence rates are found for example among agricultural workers, construction workers, nurses and cleaners [2]. In the EU, lower back pain affects more than 40% of the working population [3]. The use of a passive support around the user's trunk, i.e. exoskeletons, has been used to decrease the load on the lower back at work and also metabolic load. A passive exoskeleton, in contrast to an active exoskeleton, does not use an external power source. A passive exoskeleton uses materials, springs or dampers with the ability to store energy from human movements and release it when required. An exoskeleton may not only support but also hamper performance by increasing energy costs or affecting task execution. This can be due to a reduced range of motion, discomfort and misalignment between human anatomy and kinematics of an exoskeleton. These are several reasons why back support exoskeletons and exoskeletons in general are not widely adopted in the industry yet [4]. To improve the performance of exoskeletons, this project tries to aid the development of exoskeletons with a larger range of motion.
To develop exoskeletons, one needs to understand how an exoskeleton works. To explain this, an example of a passive exoskeleton is shown in figure 2.1, namely the Laevo exoskeleton. The Laevo exoskeleton consists of three types of pads: chest pad, back pad and two upper leg pads. When bending forward, resistance is applied at the chest and the legs due to a spring-loaded joint, generating a moment to relieve the wearer's back muscle. The chest pad incorporates rotating elements which to some degree fulfil the function of a differential transmission. Applications of this passive exoskeleton can be in a variety of fields i.e. agriculture, military, heavy industry, logistics, automotive, healthcare, warehousing and construction.

As can be seen from figure 2.1, the range of motion of this exoskeleton is mainly determined by the hip-chest support. There are also other exoskeletons with a hip-back support, as was obtained from reviewing the state of the art of exoskeletons which will be discussed later. The hip-chest and hip-back support fulfil the same function, that is to create a moment to relieve the wearer's back muscle. The difference is that the hip-chest support pushes on the chest and the hip-back support pulls on the upper back to exert a force. Most exoskeletons have almost rigid behaviour for this support so developments for torsion and lateral bending movements are desired. The objective of this thesis report is to design a hip-back support using beams for compliance in torsion and lateral bending direction while remaining stiff in the (forward) bending direction, as shown in figure 2.2. Stiffness in the bending direction is desired as this is the supporting direction. In this direction, energy is stored in a mechanism, e.g. a spring, that is connected to the beam.

Another important aspect that needs to be taken into account is that a person, wearing an exoskeleton, can move in multiple directions at the same time. Therefore, the objective is not only to achieve desired directional stiffness but also to handle a combination of deflections. This means that the design should remain stiff in the bending direction when torsional and lateral bending deflections are applied up to a certain degree. The same is true for remaining compliant in lateral bending direction when

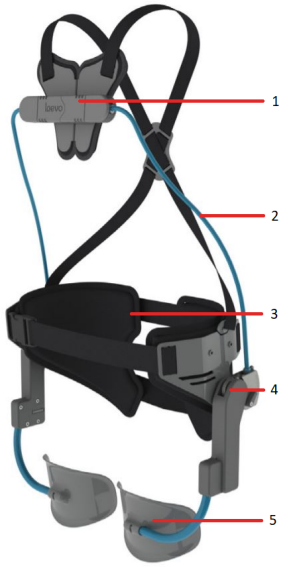

Figure 2.1: Laevo exoskeleton with highlighted parts: (1) Chest pad, (2) Hip-chest support, (3) Back pad, (4) Joint and (5) Leg pad. [5]

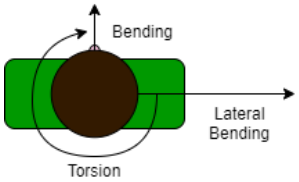

Figure 2.2: Top view of a person with highlighted (forward) bending, lateral bending and torsional directions.

torsional and bending deflections are applied to a certain extend. And lastly, remaining compliant in torsional direction when bending and lateral bending deflections are applied to a certain point. The combination of two deflections on the stiffness in the third direction is left out of scope for now.

To explain the process for the development of the hip-back support, the thesis report is structured in the following way. Chapter 3 starts with a review of comparable exoskeleton projects. In chapter 4, requirements are provided for the case of this thesis. Chapter 5 explains principle methods to change stiffness and provides multiple high-level designs within the requirements. In chapter 6, a final design is worked out using a self-developed beam optimizer. Chapter 7 explains the manufacturing of a prototype. In chapter 8 simulation tests and experimental tests are conducted and results are provided. In chapter 9, the results are discussed and in chapter 10, the thesis report is concluded.

3

Review of back supports

Before starting with the research and development of the compliant hip-back support, the state of the art of exoskeletons and exoskeleton projects was investigated. By investigating a variety of applications, this review served as inspiration to come up with a novel design. Starting with explaining how the state of the art was assembled. Then, discussing the most relevant exoskeletons that serve best for inspiration.

3.1. State of the art

The largest part of exoskeletons that aid lifting can be found in three papers that provide the overview and classification of exoskeletons [6, 7, 8]. These papers served as a basis to extend and develop the following state of the art. In these papers, it was explained how different exoskeletons are classified in categories. This classification is shown in figure 3.1. Exoskeletons are divided into three categories namely posture, active power supply and passive power supply. The last two categories are often shortened to active and passive exoskeletons. This project is scoped to passive exoskeletons. The next categorisation is about the power supply mechanism. In general, there are four different categories of power supply mechanisms namely mechanical, electrical, pneumatic and hydraulic. For the relevance of this project, mechanical power supplies are further investigated. The last categorisation is of passive mechanical power supply mechanisms. This category can be further divided in rigid beams with springs (torsional, linear, compressing, elongating, gas), compliant beams and elastic straps. For the relevance of this project, the two categories that are extended are rigid beams in combination with springs and compliant beams. These categories are most comparable to the exoskeleton that is developed for this project, so they serve best as inspiration to come up with a novel design. An overview of all exoskeletons that use rigid beams in combination with springs and compliant beams is provided below. The name of the exoskeleton, the power supply mechanism and the paper about this exoskeleton is provided.

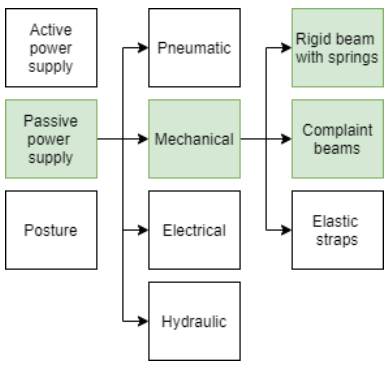

Figure 3.1: The tree diagram that visualizes the classification of exoskeletons as used in this paper.

3.1.1. Rigid beams in combination with springs

The exoskeletons with rigid beams in combination with springs are shown in appendix A.1. The main difference between the exoskeletons is that the Bending non-demand return and the Power assist suit are research exoskeletons and the Paexo back, Laevo and BackX are commercial exoskeletons. Other differences include the type of springs that are used and connections to the body.

- Bending non-demand return (BNDR) - springs - Ulrey (2013) [9]
- Laevo - linear spring - Holscher (2018) [10]
- Ottobock Paexo back - actuator based on spring - Maurice (2019) [11]
- Power assist suit (PAS) - torsion spring - Tsuzura (2013) [12]
- SuitX BackX - spring - Kazerooni (2017) [13]

3.1.2. Compliant beams

For exoskeletons with compliant beams, there are only two examples namely Virginia Tech Lowe and SPEXOR exoskeleton. For the Virginia Tech Lowe exoskeleton, flexible beams are used to store energy from bending. The SPEXOR project presents the design of a flexible beam for the back support, that allows for a large range of motion of the lumbar spine and hip [4].

- Virginia Tech Lowe - compliant beams - Alemi (2019) [14]
- SPEXOR - linear compression spring - Näf (2018) [4]

Figure 3.2: Virginia Tech Lowe's Exoskeleton in lifting configuration [14].

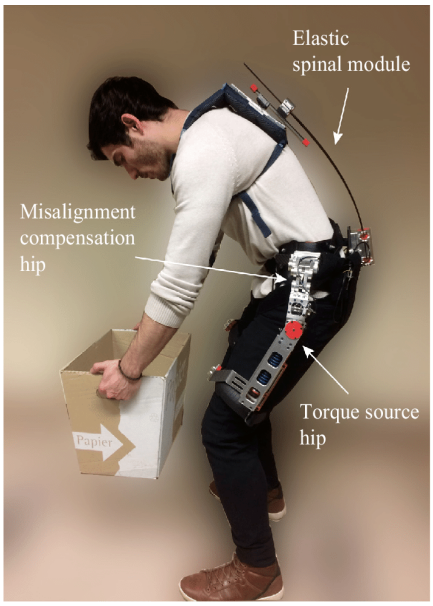

Figure 3.3: SPEXOR exoskeleton in lifting configuration [4].

The review on exoskeletons gives an understanding and classification of different concepts for exoskeletons and their working principles. In general, many papers have been written on the design and performance of different types of exoskeletons. Although, there are only two projects that enhance the range of motion for lateral bending and twisting of the upper body, namely Virginia Tech Lowe (Figure 3.2) and SPEXOR exoskeleton (Figure 3.3). The Virginia Tech Lowe exoskeleton [14], with its flexible beams for energy storage, is less comparable to the project presented in this thesis. As in this project, the goal is not to store energy in a different form but to develop an exoskeleton purely for improved range of motion. The other project that was found was the SPEXOR exoskeleton. The SPEXOR exoskeleton presents the application of a flexible spinal module to allow for a large range of motion of the upper body [4]. In the SPEXOR paper, a comparison was made between an elastic

and a rigid spinal module by measuring perceived task difficulty. The paper concludes that an elastic spinal module improves range of motion and decreases task difficulty. This illustrates the relevance of developing a compliant support for this thesis. The main difference between the project for this thesis and the SPEXOR project is that the SPEXOR project is more focused on gathering anatomical and user experience data by using a random flexible support. The purpose of the project presented in this thesis is to show multiple solutions and work out the best solution for a compliant hip-back support with specified directional stiffness.
Concluding on this review, there are not many compliant exoskeletons that improve the range of motion. For rigid beams in combination with springs, no applications of improved range of motion were found. However, investigation of exoskeletons with compliant beams did propose one promising concept with improved range of motion. This was the SPEXOR project which described the relevance of developing a compliant concept to reduce task difficulty. This review did not provide any novel designs that can be used for inspiration. So, the next step to develop a compliant concept is to use a suitable design method for compliant mechanisms to reach the specific stiffness characteristics. However, before a design can be developed, the requirements for this thesis are specified.

4

Case analysis

To achieve the objective of this project, designing a compliant hip-back support with specific directional stiffness, requirements need to be specified. The design was applied to a case of the wearable robotics project. The wearable robotics project [15] is a government-funded research project that helps to develop wearable robotics for people to regain and strengthen their movements. In the wearable robotics project, multiple research projects are investigated, e.g. wrist supports, neck supports and back supports. Various researchers, e.g. from the Delft University of Technology, work on this project to research and develop new idea's that can be applied in the future.

In this thesis, the goal was to improve the original design of a back support of the wearable robotics project, which is shown in figure 4.1. The material of the original support is a structural steel with a Young's modulus of 210 GPa and shear modulus of 76.9 GPa. The cross-section of the beam has a thickness of 5 mm and a varying width between 20 and 29 mm. The weight of the current hip-back support is 0.98 kg. The original support is relatively stiff in all directions and that needs to be improved. The support can be developed completely different than the original support as long as the design is within requirements, which are specified in the next section.

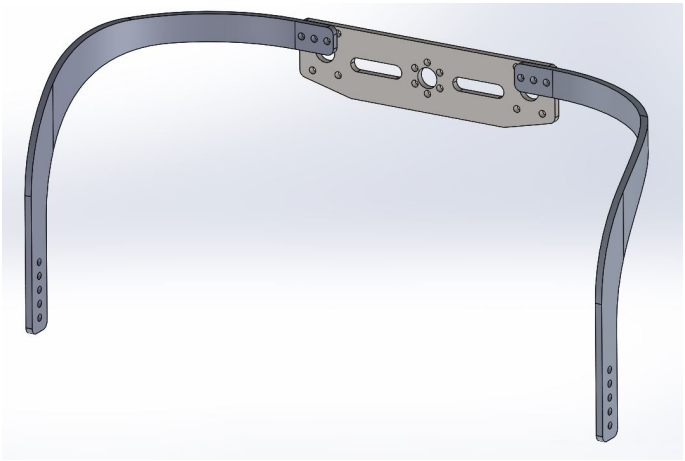

Figure 4.1: Original back support from the wearable robotics project [15].

4.1. Requirements

The requirements for designing a compliant hip-back support are as follows. A human body with twist axes, shown in figure 4.2, presents the rotations around three principle axes in the body. On the human body, a force needs to be transferred via a compliant mechanism from thighs to the upper back where the energy from bending is stored. To specify the last statement in more detail, bullet points are formulated. After this dimensional and stiffness specifications are provided.

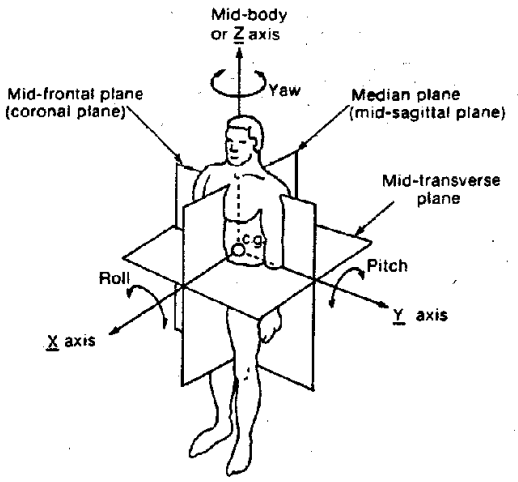

Figure 4.2: Principle twist axis where a human bends about and with the center of gravity in the middle [16]. The axes define the orientation of the coordinate system used in this thesis. The position of the origin in specified later in this thesis.

- The support is connected at two points, one at each hip. These points are connected via a compliant beam to the upper back.
- The support should be relatively stiff in forward bending and relatively compliant in lateral bending and torsion.
- The support should be symmetrically stiff in lateral bending and torsion.
- Support should not hinder freedom of arms and should follow the human body to form an inconspicuous back support.

4.1.1. Dimensions

The requirements for the dimensions are based on anthropometric data and the dimensions of the original back support. The anthropometric data from [17] provided the average sizes of a human. Based on the locations of the back pad and connection to the hip of the original support, the support should follow the following path. Starting from point (0,0,0) m at the hip and following an elliptical path to point (0.15, 0.20, 0.20) m at the upper back. Then the support will follow a symmetrical path back from (0.15,0.20,0.20) at the upper back to (0,0.4,0) at the other hip. Setting up this design space requirement will lead to an inconspicuous support that is low profile and follows the human body.

4.1.2. Stiffness

To determine the stiffness requirements, forces and deflections are specified. The torque and forces are determined based on experimental data from the wearable robotics project. The hip-back support should be able to handle the following forces and moments. The torque is 65 Nm around the X, Y and Z axes shown in figure 4.2. That means that for a height of 0.2 meters, the forces on the support are 325 N in the X and Y direction at the point connected to the upper back.
The desired deformation range for lateral bending is 30 degrees to both sides around the X-axis shown in figure 4.2. The desired deformation range for twisting is 30 degrees around the Z-axis shown in figure 4.2. This was an estimation for a desired range of motion. The deformation range for bending should be minimal. This means that energy from bending is stored mostly in the power supply mechanism, e.g. a spring. For now, the following arbitrarily requirement is chosen that moving 30 degrees in lateral bending and torsion should result in a maximum of 3 degrees in bending, for the same applied torque. This 3 degrees rotation is in the forward bending direction and around the Y-axis shown in figure 4.2. The resulting displacement of the middle point, with the specified height of 0.2 m, is 10 mm deflection in forward bending direction and 100 mm deflection in the lateral bending direction.
The desired directional stiffness can now be determined based on the data above. For forward bending, this results in a stiffness of 32.5 N/mm. For lateral bending, the desired stiffness is 3.25 N/mm. Lastly, for twisting the desired stiffness is 124.1 Nm/rad.

5

Concept Generation

The review of back support projects did not provide any novel applications of directional compliance to improve range of motion. Therefore, the next idea was to investigate suitable design methods for compliant mechanisms to reach the specific stiffness characteristics. To better understand the field of compliant mechanisms and specifically stiffness, a literature review was conducted on stiffness characterization methods for compliant mechanisms [18], which can be found in appendix A.10. The review provided one promising method to develop a compliant structure with desired directional stiffness, namely the Freedom and Constraint Topologies method.

5.1. Freedom and Constraint Topologies

To find a compliant mechanism design with specific freedom and constraint directions, a synthesis method called Freedom and Constraint Topologies (FACT) can be applied. This method is often used by designers to develop early-stage flexure system designs, with specific compliant and stiff directions, via “paper and pencil sketches” [18]. The FACT method enables designers to visualise the regions wherein all compliant constraint elements could be placed that would allow the mechanisms desired degrees of freedom (DOFs). Applying the FACT method, a leaf flexure design (Figure 5.1) was obtained for the desired directional stiffness characteristics of this project. The leaf flexure connects a fixed and free point where the free point has one stiff bending direction, one compliant bending direction and a compliant torsional direction. When this concept is applied to the design of a compliant hip-back support, this results in the required directional stiffness, i.e. stiffness for forward bending, compliance for lateral bending and compliance for twisting. Therefore, the overall support should model the desired stiffness behaviour closely and thus should achieve the objective. Next, the design for this leaf flexure is developed based on the provided requirements.

5.1.1. FACT Design

As explained in section 5.1, using the FACT method, a design based on the leaf flexure concept needed to be developed. For estimating the values for the thickness and width of this design, linear formulas for small force-deflection behaviour were used. These are the so-called forget-me-not formulas [19] that are used to determine parameters, e.g. deflections, forces and dimensions, for the bending of beams in different configurations. Even though these formulas are applied to relatively small deflections in the elastic limit, it was investigated if they could relatively closely predict the cross-sectional dimensions of the leaf flexure for larger deflections. The accuracy was checked by FEM simulations on the results from these formulas. Three formulas are provided for bending, lateral bending and torsion.

Bending:

$$\delta_x = \frac{F_x L^3}{3E\frac{tw^3}{12}} = 0.01 \tag{5.1}$$

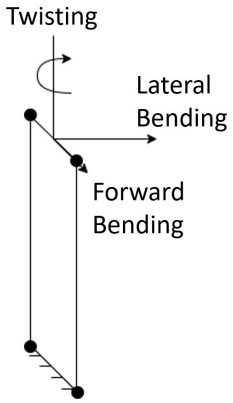

Figure 5.1: Sketch of a leaf flexure with one stiff bending direction (forward bending), one compliant bending direction (lateral bending) and a compliant torsional direction (twisting).

Lateral bending:

$$\delta_y = \frac{F_y L^3}{3E\frac{wt^3}{12}} = 0.1 \tag{5.2}$$

Torsion:

$$\theta_z = \frac{T_z L}{G\beta w t^3} = \frac{30}{180}\pi \tag{5.3}$$

where

$$T = F * L \tag{5.4}$$

Values for parameters are obtained from the specified requirements and a value for β was iteratively determined. This resulted in a thickness of 3.5 mm and a width of 11.2 mm. This means that the cross-section ratio, which is the thickness to width ratio, is approximately 1 to 4 for a beam with a length of 200 mm.

To verify if the forget-me-not formulas were accurate, FEM solid modelling was carried out. For the simulations, a commercially verified software was used, namely ANSYS Mechanical®. The extensive results and simulation details can be found in the appendix A.2. For bending, the results from the forget-me-not formulas were within 5 % of the results from FEM modelling. This was expected as the deflections were relatively small. For larger deflections in torsion and lateral bending direction, the results were less accurate. For lateral bending, the results were 13% off and for torsion, the results were 267% off. For the sake of getting an estimation for a leaf flexure design, these results were satisfying, even though the results were not completely correct. Also, the large inaccuracy for torsion was a desired result as this indicates a lower stiffness for twisting.
An important note is that simulations showed that the stresses inside the material were larger than the yield strength. Based on this, the conclusion can be drawn that the material will deform plastically for these large deformations. Therefore, setting less ambitious force or deflection requirements or changing material can help the structure to remain in the elastic region.

One last step is needed to complete the design of the leaf flexure. Currently, the leaf flexure design is not yet connected to the hips. To complete the leaf flexure design, a support beam needed to be developed to connect the hips. For simplicity's sake, the support beam is assumed to be rigid in all directions so the only compliance behaviour is obtained by the leaf flexure. To develop a rigid supporting beam, two arbitrary examples of cross-sections are a square and circular cross-section. For a beam with the same weight, the circular beam has less angular and bending deflection. Therefore, the circular cross-section is desired and resulted in the design shown in figure 5.6. This design is a satisfying solution with desired directional compliance within requirements when a single deflection is applied. However, this might not be the case for a combination of deflections also called coupled motions.

When a leaf flexure is subjected to a combination of rotation and forward bending, the stiffness in forward bending direction decreases dramatically. This phenomenon is not desired as the goal of this project was to remain stiff in the bending direction for a combination of deflections. To visualize stiffness behaviour for coupled motions of the FACT design, multiple simulations were executed and can be found in appendix A.2.1 and A.2.2. The simulations for coupled motions of twisting and forward bending show a decreased forward bending stiffness. However, it is important to note that this decreased bending stiffness is much less significant when the leaf flexure is relatively thick. This means that the FACT design is satisfying as the decreased bending stiffness is not significant. The disadvantage of this concept is that it is relatively bulky. The reason for this is because the underlying idea behind this concept is to divide this rather complex kinetostatic task into a stiff planar design and a compliant leaf flexure design. The stiff planar beam can be modelled as a rigid cantilever beam and the compliant leaf flexure as a cantilever beam that can reach relatively large deflections. These design problems can be solved rather quickly and can be improved using different cross-sections and materials, e.g. composites, for the best stiffness behaviour. The next section investigates how to improve stiffness behaviour of the leaf flexure concept for coupled motions. For this purpose, methods to change stiffness on demand were investigated.

5.2. Stiffness change on demand

To improve the stiffness behaviour of the leaf flexure for coupled motions of twisting and forward bending, research was conducted on ways to change stiffness on demand. The only four categories that exist to change stiffness on demand were investigated [20]. These categories are shape, material, boundary condition and prestress. Within these categories, some promising concepts are explained that can be applied to the case of this thesis. All the concepts are based on the FACT design.

5.2.1. Shape

First, changing stiffness based on shape. This comes down to changing the form of an object. Examples of shape-changing structures to control stiffness on demand are origami and multi-stable structures. Origami is the art of folding paper. However, its working principle is not limited to folding paper, which led to new, origami-based, engineering solutions in a variety of fields. An example is shown in figure 5.2, where the foldable paper design led to a foldable structure of solar panels for space applications. Multi-stable structures have multiple potential energy wells where the shape of the structure is stable. Applying a high enough force can make this structure change form and remain stable in another potential well.

A design solution based on shape for a hip-back support was conceptualized using origami. The next self-developed idea is similar to the leaf flexure design. It has a rectangular cross-section with the same dimensions as the leaf flexure design. The difference is that this self-developed origami concept can fold open. When torsion is applied to this beam, the rectangular section folds open into 4 smaller rectangular sections that together form a hollow square. This design is shown in figure 5.7. Now, this design has stiffness in the forward bending direction when the body is twisted. However, it now also has stiffness in the lateral bending direction. Another disadvantage is the feasibility of the compliant hinges. Many cycles with these hinges will result in fatigue of these compliant hinges.

5.2.2. Material

Second, changing stiffness based on material comes down to changing the substance or mixture of substances that form an object. Examples of stiffness changing structures are shape memory polymers, optimized fiber-reinforced composites and materials that change stiffness based on thermal, magnetic or electrical actuation. Shape memory polymers are polymer structures that return to an original shape when for example heat is applied. Optimized fiber-reinforced composites can be used to generate the ideal stiffness solution for each element in a structure for single deflections and a combination of deflections. Structures, with controllable elements, can change local material properties such as stiffness. This gives direct control over the structure but actuation must be applied precisely. An

example is shown in figure 5.3 where the stiffness of the structure is controlled locally by heat actuation.

A design solution based on material for a hip-back support was conceptualized using the controllable structure concept. Creating a structure where stiffness of each element is controllable can improve overall stiffness behaviour at any moment. However, understanding in which elements when to actuate is needed to create desired directional stiffness. Moreover, a control system is needed to precisely actuate specific elements. Working out this concept would focus more on precise actuation of elements by building a control system instead of achieving desired directional stiffness using beams.

5.2.3. Boundary Condition

Third, a boundary condition is a contact support where deflections are prohibited by a rigid outside design. At a certain point of deflection, the structure will come in contact with the rigid support and stiffness increases. Within a specific range, deflections are free and this is applied in flexure hinges for example. An example of a flexure hinge is shown in figure 5.4.

The self-developed concept based on boundary condition is shown in figure 5.8. A compliant hinge is designed with contact support points that prohibit lateral bending and twist after 30 degrees deflection. The outside design is calculated such that there is a contact support for lateral bending from 30 degrees and for twisting from 30 degrees. This is also true for a combination of twisting and lateral bending of both 30 degrees. The advantage of this design is that it meets the requirements. However, this leads to a relatively heavy system. Another issue that can occur is fatigue due to the relatively large deformations and many cycles that the compliant structure is subjected to. For this boundary condition design, the compliant beam is replaced by a compliant hinge to model the stiffness behaviour.

5.2.4. Prestress

Last, changing stiffness based on prestress comes down to structures that are internally stressed to for example counterbalance a force that will be introduced on the structure. Two contrastressed structures that are joined can create interesting behaviours like zero-stiffness structures. This would not have been possible without prestress in the joint structures. To better explain this, in figure 5.5, an example is shown. An I-beam is shown that can achieve zero stiffness for torsional behaviour [24]. To explain how this is possible, it is needed to explain how this I-beam is constructed. Two curved flanges are separated first and then glued to the web. Since these flanges were originally curved, this creates internal stress in the structure. This internal stress leads to interesting stiffness behaviours. For the concept shown in figure 5.5, it led to a bistable structure but changing the layup can allow for zero-stiffness behaviour.

For self-developing a prestress design, inspiration is taken from the concept proposed by Lachenal [24]. The underlying idea behind this self-developed concept is that the prestress improves stiffness behaviour for coupled motions. To adapt the concept proposed by Lachenal [24], to a design within requirements for this case, the first step is to create a solid web. The second step is to reduce the width of the flanges to the thickness of the web. This is to achieve the desired directional stiffness for single deflections. The thinner flanges need to be curved and then connected to the web. This is shown in figure 5.9. It is unknown if this self-developed concept has better stiffness behaviour for a combination of deflections. This can only be determined by developing different prototypes with varying dimensions. This is because no modelling software is available that can simulate the effect of prestress on the stiffness of a structure. This also means that no simulations can be done to obtain satisfying results.

5.3. Concept evaluation

A variety of self-developed designs were proposed to adapt the leaf flexure concept to improve directional stiffness behaviour for a combination of deflections. The designs were all based on the rectangular beam concept that was synthesised using the conventional FACT method. The issue was that the designs were relatively bulky compared to their output range of motion. To decrease bulkiness, shape optimization was investigated to include the complete structure in the output range of motion and handle the complex kinetostatic task.

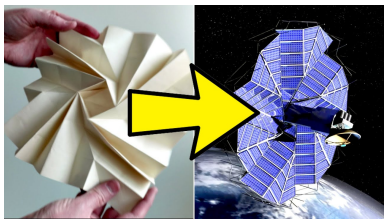

Figure 5.2: Shape; using origami to go from a foldable paper on the left to solar panel deployment for space applications on the right [21].

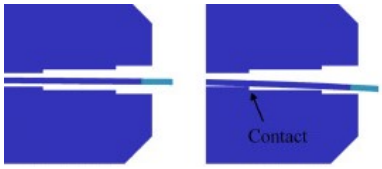

Figure 5.4: Boundary condition; flexure hinge that is constraint by outside design [23].

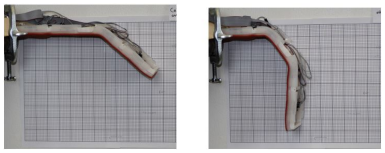

Figure 5.3: Material; using heat actuation to increase the stiffness for elements of the structure [22].

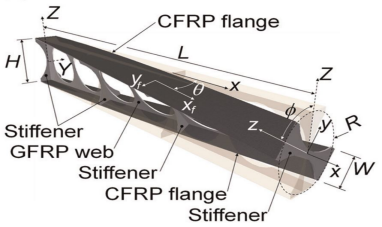

Figure 5.5: Prestress; Stressed flanges separated by a web to create a zero-stiffness or bistable structure [24].

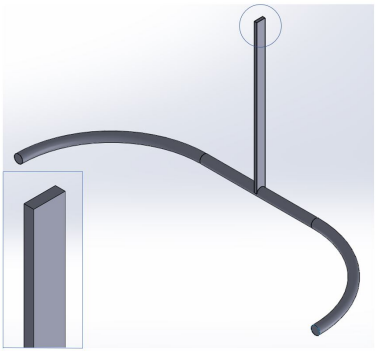

Figure 5.6: Self-developed FACT concept with a compliant rectangular beam and a rigid circular support.

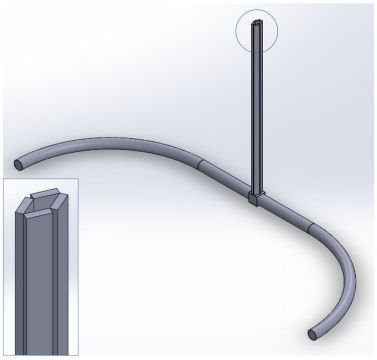

Figure 5.7: Self-developed origami concept which is a rectangular shape that can fold open using compliant hinges.

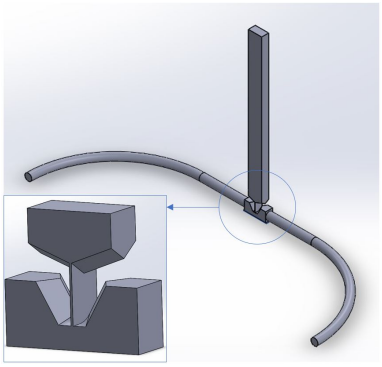

Figure 5.8: Self-developed boundary condition concept where sideways deflection and twisting is possible to a maximum of 30 degrees.

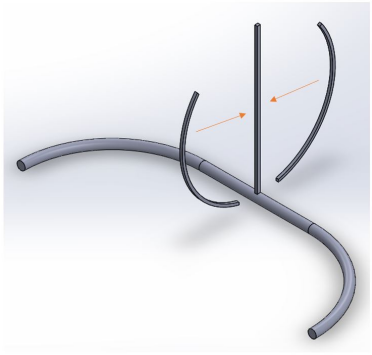

Figure 5.9: Self-developed prestress concept where two curved flanges are separated by a web. To complete this design, the flanges need to be connected to the web.

6

Optimization

6.1. Introduction

The previous chapter did not provide an ideal solution to the case of this project. When a designer does not have a particular shape in mind, optimization techniques can be used to generate the desired solution. To augment the designer's intuition and develop novel solutions, optimization can generate solutions that the designer might not have come up with by using conventional synthesis methods for compliant mechanisms, like the FACT method. It is intended to predict the best structure for a particular design problem. Shape optimization was selected to come up with a less bulky shape compared to the output range of motion. The cross-section was set to be constant to retrieve structure that could be fabricated using e.g. bending machines and not be limited to layer additive manufacturing as this reduces material selection. This kind of shape optimization is not available in commercial FEM optimization software. Generally, commercial FEM optimization software is used for example to remove material at specific locations where there is less stress for a specific input force. For this thesis, a novel so-called parametric shape optimization is used where the beam path and cross-section are optimized to reach specific kinetostatic behaviour. Since there was no commercial software available with this ability, a home-developed tool [25] was adapted to the case of this thesis. A modification was required as the original code was only able to generate an optimized structure for a cantilever beam and could not optimize for an angular deflection for a given input moment. This made the original optimizer not directly applicable to the case of this thesis. In the next section, the process of optimization of the beam shape is elaborated including the extensions that were made. After that, results are generated with the extended optimizer and verified by simulations.

6.2. Optimization of the beam shape

For this thesis, the goal was to reach specific directional stiffness behaviour and optimizing geometrical parameters of the beam. These parameters were the spine shape of the beam, cross-section and orientation of this cross-section. For this optimization process, the definition of requirements, objective function, optimization settings and the finite element solver are explained. For each part, where the original optimizer was extended, the changes are elaborated in more detail.

6.2.1. Topology

First, information on the beam path parameters is specified. The beam is a double-clamped beam, thus fixed at the two endpoints, that is loaded in the middle point. The position of the grounding points is chosen based on the dimensional requirements where endpoint 1 is positioned at X_{e1}=0m, Y_{e1}=0m, Z_{e1}=0m. Endpoint 2 is positioned at X_{e2}=0m, Y_{e2}=0.4m and Z_{e2}=0m. The loaded middle point is positioned at X_m=0.15m, Y_m=0.2m and Z_m=0.2m.

The original optimizer could only optimize cantilever beams. To extend the optimizer to solve for a double-clamped beam, the number of beam elements was changed from $nbeam$ to $2 * nbeam - 1$. For plotting the undeformed configuration of the double beam, a single beam was plot and mirrored as

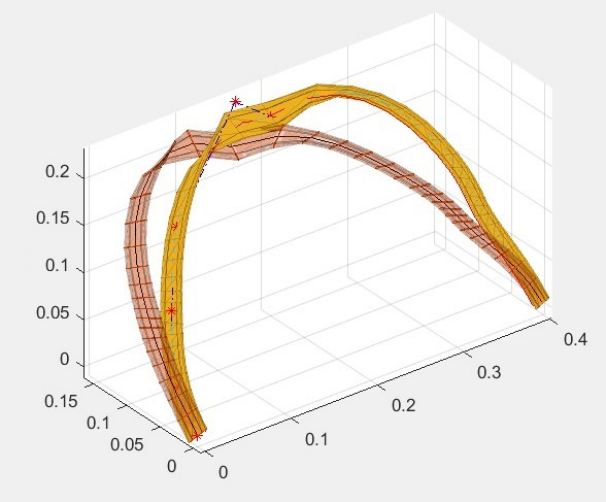

Figure 6.1: Twisted middle part due to the mirroring of the single beam shown in undeformed configuration (orange) and deformed configuration (red).

can be seen in appendix A.8 line 79 till 81. This did not result in a continuous beam as the middle part was twisted, which can be seen in figure 6.1. To generate a continuous beam, the orientation of the middle point was manually flipped 180 degrees. This is explained in line 108 till 111 of appendix A.8. To constrain the endpoints and model them as fixed supports, line 162 and 163 of appendix A.8 were added.

6.2.2. Objective function

For shape optimization, the objective function is defined for three specific cases of resulting deformations under loadings. The objective function considers the error between the actual deformation and the set desired deformation of the free middle point. The optimizer tries to minimize the objective function by optimizing for different shape-related parameters along the beam. In the first case, the applied force of 325 N in bending direction should result in a displacement of 10 mm in the x-direction. In the second case, the applied force of 325 N in lateral bending direction should result in a displacement of 100 mm in y-direction. In the third case, the applied moment of 65 Nm should result in an angular deflection of 0.5236 radians around the z-axis. The stiffness behaviour for lateral bending (y-direction) and twisting (θ_z-direction) is desired to be symmetrical which leads to the following formula for the objective function

$$f_{tot} = f_x + f_y + f_{\theta_z} = (0.01 - dx) + |0.1 - dy| + |0.5236 - d\theta_z| \tag{6.1}$$

where dx and dy are displacements in the two coordinate directions and d_{θ_z} is an angular deformation around the third coordinate direction.

Optimization for an angular deflection $d\theta_z$ for an applied moment was not straightforward. This was because angular deflection was calculated at each timestep, e.g. between the last and second to last timestep. Extending the code by summing all the angular rotations for each time step is explained in line 196 to 206 of appendix A.8. The next step is to set the objective function based on this summation and this is explained in line 18 to 21 of appendix A.9. In appendix A.9, the complete objective function based on equation A.9 can be found with specified forces, moments and deflections.

6.2.3. Parameter optimization

In this work, the parameter optimization is divided into two categories to form the beam. The first set is cross-section parameters and orientations along the beam. The second set is parameters related to the spine shape of the beam.

For the cross-section, an I-beam was chosen as its dimensions enable a large variety of combinations that describe the cross-section. Optimization using an I-beam cross-section enables convergence to multiple other prevalent sections like H, T, rectangular or square-shaped cross-sections. The

I-section is defined by web height H, flange width B, flange thickness h, web thickness b, and the orientation ϕ. The first four parameters are optimized once for the complete beam to make the generated shape extrudable. Then, the orientations are optimized on five control points along the beam with the other orientation being interpolated in between based on the five points. For the final design, the I-shaped cross-section converged to a rectangular-shaped beam so this section is also defined. The rectangular-shaped section is defined by height H, width W and orientation ϕ.
For all mentioned parameters, lower and upper bound constraints were added to limit the optimizer to come up with reasonable dimensions within the design space without crossing itself. Also, bounds were added to keep the I-shaped cross-section through the beam and avoid a full twist.

For retrieving the most suitable spine shape, a beam shape parametrization scheme was developed using a B-spline. B-splines have knots that are distant from each other and are used for curve-fitting and numerical differentiation of experimental data. This is used to shape the beam in three dimensions. Also, a constraint was added to the spine shape. The beam should follow a 2D elliptical path that is based on average human body sizes. This is such that the support follows the human body to be inconspicuous. This path can be defined as a planar constraint equation formulated as

$$\frac{x^2}{0.15^2} + \frac{(y-0.2)^2}{0.2^2} = 1 \tag{6.2}$$

An important note is that this equation reduces the three Cartesian coordinates to two free coordinates since x or y can be derived using this constraint equation.

6.2.4. Optimization process and numerical model

The B-spline which was used to form the spine shape is based on optimized control points. The spline is a degree-four with knots determined based on the de Boor algorithm [26].

To determine the large displacements due to multiple loadings, a large deformation finite element solver was employed which uses geometrically non-linear co-rotational beam elements introduced by Battini [27]. One important aspect of the solver that needs to be elaborated is beam modelling. For different structures, different modelling techniques are suitable. The different modelling techniques are shown in figure 6.2. In general, 1D beam modelling is most accurate for relatively thick structures as in-plane deformations are suppressed. 2D shell modelling is generally most accurate for thin-walled structures and 3D solid modelling is most accurate for all type of structures. However, 1D beam modelling is the fastest technique and the time to solve increases exponentially using 2D shell modelling. Time also increases exponentially for using 3D solid modelling instead of 2D shell modelling. To decide if beam modelling was accurate for the case of this thesis, an estimation had to be made on the resulting structure. In chapter 5, the FACT method provided a shape with a cross-section ratio of 1 to 4. Therefore, it was expected that using 1D beam modelling would lead to a satisfying solution.

To optimize the parameters, the Multi Start option from the MATLAB®optimization toolbox is used. For this option, the fmincon is used as a function with the interior-point as the algorithm set. The Multi Start optimizer uses five random starting points for the parameters to optimize for.
Lastly, the material constants that are used are a Young's modulus E = 200 GPa and a shear modulus G = 76.9 GPa.
Now the optimizer is fully explained, the next step is to obtain results.

6.3. Results of optimization

The requirements from chapter 4 were set as input parameters for the developed optimizer. The Multi Start ran multiple times for different bounds but no satisfying results were obtained. It seemed that these requirements were too ambitious to retrieve an optimized beam. So research was conducted changing the height, applied torque, cross-section and deflection specifications to achieve results that were almost within the requirements. An overview of this is shown in figure 6.3.

Two input parameters, namely height and force, are researched and their influence on the deflection for forward and lateral bending. In the first row, the reduction of height from 500 mm to 350 mm to 200

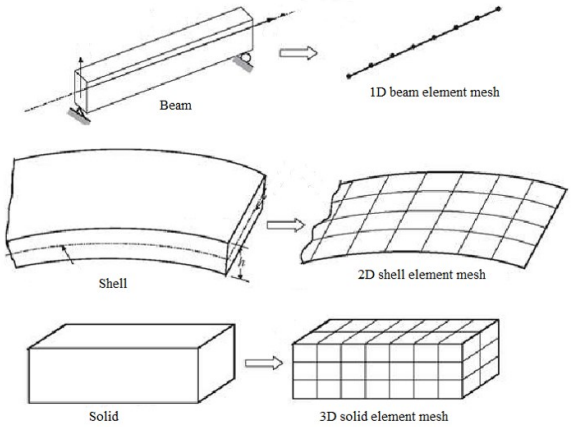

Figure 6.2: Different modelling techniques to model elements of a structure in three dimensions. Beam modelling stores thickness and width of the cross-section. Shell modelling stores the thickness of the cross-section. Solid modelling provides the stress throughout a part.

Height

Height = 0.5m	Force = 162,5 N	CS = I-beam
Displacement	**0.25x0.03m**	0.125x0.015m
Results	**51 degrees**	21 degrees

Height = 0.35m	Force = 162,5 N	CS = I-beam
Displacement	0.17x0.03m	0.09x0.015m
Results	85 degrees	32 degrees

Height = 0.2m	Force = 162,5 N	CS = I-beam			
Displacement	0.08x0.015m	0.07x0.01m	0.06x0.01m	0.05x0.025m	0.05x0.01m	0.05x0.00625m
Results	ERROR	ERROR	ERROR	78 degrees	74 degrees	41 degrees

Force

Force = 129,6 N	Height = 0.2m	CS=Rectangle
Displacement	0.06x0.0125m	0.05x0.00625m
Results	ERROR	36 degrees

Force = 162,5 N	Height = 0.2m	CS=Rectangle		
Displacement	0.1x0.015m	0.07x0.01m	0.06x0.01m	0.05x0.00625m
Results	ERROR	ERROR	ERROR	44 degrees

Force = 203 N	Height = 0.2m	CS=Rectangle		
Displacement	0.06x0.01m	0.06x0.015m	0.05x0.01m	0.05*0.00625m
Results	ERROR	ERROR	37 degrees	ERROR

Force = 244 N	Height = 0.2m	CS=Rectangle		
Displacement	0.07x0.015m	0.6x0.1m	0.05x0.01m	0.05x0.00625m
Results	ERROR	30 degrees	27 degrees	ERROR

Force = 325 N	Height = 0.2m	CS=Rectangle		
Displacement	0.07x0.015m	**0.06x0.01m**	0.05x0.01m	0.05x0.00625m
Results	ERROR	**24 degrees**	53 degrees	ERROR

Figure 6.3: Results from optimization for multiple height, force, cross-section and deflection specifications. The first and second row is research on the effect of height on the deflection specifications. The third, fourth and fifth row are research on the effect of force on the deflection specifications.

mm is shown and the influence on the deflection specifications. In this research, an I-shaped cross-section and an applied force of 162.5N are used for input specifications. The results show the angular deformation when the run was successful. The results showed an error when the goal function was too ambitious. From this research, it can be drawn that the height of the beam influences the maximum possible deflection of the beam for lateral bending. Besides, a larger stiffness ratio could be achieved using a larger height. An example of a resulting structure from this research is shown in figure 6.4. This example is also marked as bold in the top row in figure 6.3.

This beam had a deflection of 30mm in forward bending direction with a corresponding directional stiffness of 5.4 N/mm. The deflection in lateral bending was 250 mm with a corresponding stiffness of 0.648 N/mm. That is a relative stiffness of 8.333 to 1 for an applied force of 162.5 N in both directions. The angular deflection was 51 degrees for twisting and a corresponding rotational stiffness of 75 Nm/rad for an applied torque of 65 Nm. The height of the beam was 500 mm.

The next research topic was about the influence of force on the deflection specifications. The results from this research are provided in the second and third row of figure 6.3. For this research, a rectangular cross-section was used instead of a I-shaped cross-section. This was because the I-shaped cross-section from the height experiment started to resemble a rectangular shape. For the research on the influence of force on the deflection specifications, the force was increased starting from 129.6N

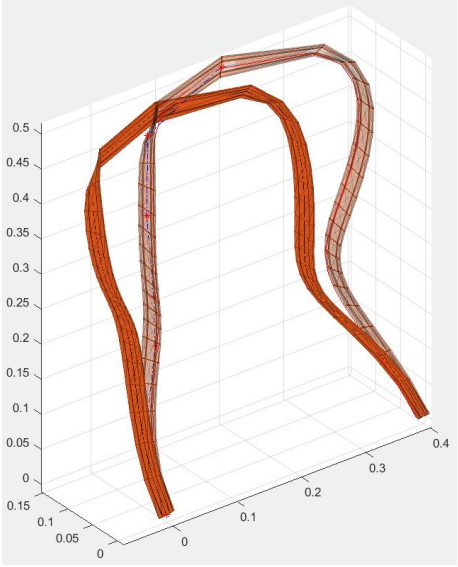

Figure 6.4: Isometric view of beam design that yielded desired solutions. The deformed (full color) and undeformed (light color) configuration are plotted.

and gradually increased to 325N. The results show that the increasing force does not influence the displacement specifications much.

For this thesis, it was selected that the height of the beam was more important than the relative stiffness of the beam. Because then, this design could be applied to the case of the wearable robotics project. For now, it was chosen that a lower relative stiffness was satisfying. This resulted in the final structure that is marked bold in the bottom row of figure 6.3. This design had a thin rectangular cross-section with dimensions 27.5mm by 1.5mm and is shown in figure 6.5. This resulted in a deflection of 60 mm by 10 mm for the applied force of 325 N and 24 degrees for the applied moment of 65 Nm. The corresponding stiffness is 32.5 N/mm in forward bending direction, 5.4 N/mm in lateral bending direction and 155 Nm/rad rotational stiffness for twisting. It was interesting to realize that the resulting structure was different from the structure obtained via the FACT method. This shows that optimization techniques are useful to develop novel solutions when a designer does not have a particular shape in mind. Using optimization, a solution was generated that the designer did not come up with by using other conventional synthesis methods. The next step was to verify this design using a commercial FEM software, namely ANSYS Mechanical®.

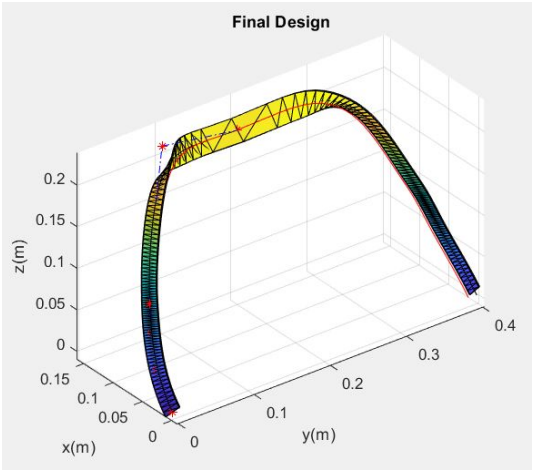

Figure 6.5: Selected final design in undeformed configuration with relative stiffness of one to six for forward bending relative to lateral bending.

6.4. Verification optimizer

A static structural analysis was conducted using structural steel as a material. The model was imported as a .SAT file to have a working structure in ANSYS Mechanical®. From then on, a mesh could be created using solid modelling. As explained earlier in section 6.2.4, solid modelling is the most complex but also the most accurate modelling technique to find the best approximations for deflections. After a mesh was generated, the fixed supports were added to the endpoints of the beams. The option for large deformations was turned on in the solver controls for analysis settings. An applied force of 325N lead to a deformation of 41 mm in bending direction and 69 mm in lateral bending direction. This is shown in figures 6.6 and 6.7. The deflections are measured using directional deformation. The resulting stiffness for forward bending direction is 7.93 N/mm and for lateral bending 4.71 N/mm. The moment of 65 Nm led to an angular deformation of 31 degrees. This is shown in figure 6.8. The resulting rotational stiffness for twisting is 120 Nm/rad. The mass was retrieved from the table of geometry properties and was 0.259 kg. The final design was specified and will be manufactured in the next chapter.

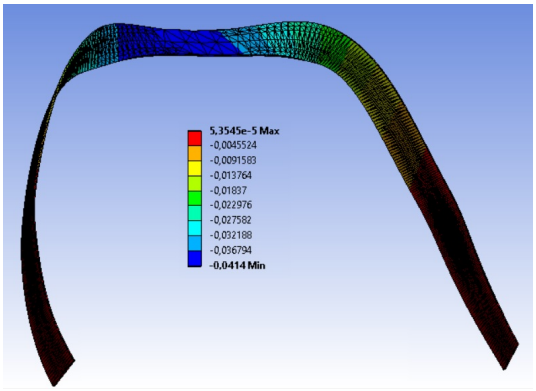

Figure 6.6: Forward bending deflection for an applied force of 325N measured using ANSYS Mechanical®.

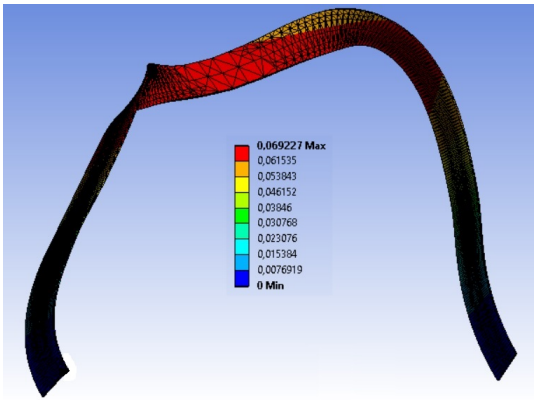

Figure 6.7: Lateral bending deflection for an applied force of 325N measured using ANSYS Mechanical®.

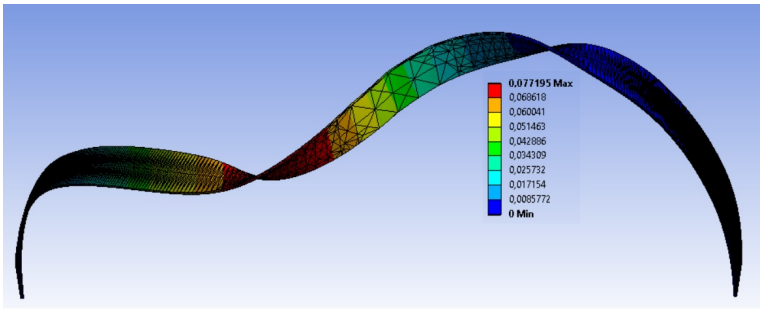

Figure 6.8: Topview of the structure providing total deflection for an applied moment of 65Nm for torsional bending measured using ANSYS Mechanical®.

7

Manufacturing

The design that was generated in the previous chapter was not straightforward to manufacture. To produce this complex 3D-curved rectangular beam, different manufacturing methods were investigated. This investigation is further explained in appendix A.3. To fabricate a satisfying approximation of the optimized design, a strip was laser-cut which was extracted from flattening of the spatial shape. The next steps were to use roll bending to create the 3D curved beam and to manually apply a twist in the middle of the beam. Now, the method to create the structure is clear. The next step was to make the manufacturing plan in more detail for the prototype and selecting a material. After this, the process of manufacturing the prototype is elaborated.

7.1. Manufacturing Plan

To have a design that can be laser-cut, the 3D shape needs to be converted to a strip. The shape in MATLAB® was exported as a .STL file and imported in SolidWorks®. This imported file in SolidWorks® was a set of surfaces that needed to be closed and knit together to create a solid. To create a smart structure where the middle part could be twisted, the points on the solid were connected using the 3D sketch tool. The lines that were created, by connecting the points, were used to create a swept boss/base. Using the right lines as guide curves made it possible to create the untwisted structure. This untwisted structure is shown in grey in figure 7.1.

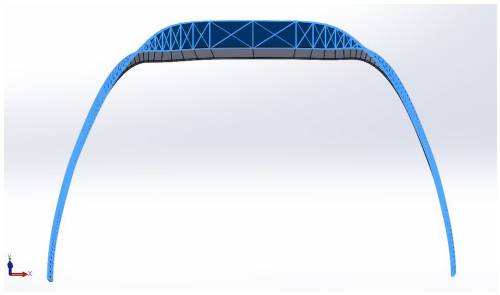

Figure 7.1: Final beam design is shown in blue and untwisted beam design shown in grey shown in SolidWorks®.

After this untwisted solid was created, the next step was to flatten this solid. The top surfaces on the structure were selected and the function flatten from the sheet metal module was used to create a strip. This strip was exported into a drawing and send to the laser-cutter to create the physical part. The model can be laser-cut on full scale using a plate of 1.5x75x750mm. This can be seen in figure 7.2. After the strip was laser-cut from the plate, roll bending needed to be applied to get the exact arc of the beam. This is shown in grey in figure 7.1. The last step is to apply a twist to the middle plane to get the final shape. The final shape is shown in figure 7.1 in blue. Now, the steps of producing the beam are shown in SolidWorks® and the manufacturing plan is clear, the material to produce the beam was selected.

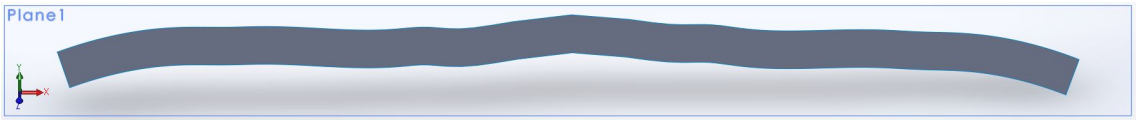

Figure 7.2: Top view of the curved strip to laser-cut, shown in SolidWorks®.

7.1.1. Material

For these type of large structures that have to handle relatively high forces and large deflections, it was estimated that spring steel was the most suitable material. Spring steel has suitable stiffness characteristics and can achieve large deflections, up to a certain degree, without deforming plastically. Spring steel has a relatively large region of elastic deformation because the yield strength is relatively high. To better understand the stiffness behaviour for spring steel and understand how to produce a prototype using spring steel, experiments were conducted on three strips of spring steel with different thicknesses. This investigation can be found in appendix A.4. Even though spring steel is a promising material, it is relatively expensive. Since the scope for this thesis was not to create a fully functioning compliant hip-back support for a commercial exoskeleton but a proof of concept was satisfying, stainless steel was selected as the material for manufacturing the beam. This was to create a cheap prototype and to understand if the stiffness behaviour was desired. The stiffness behaviour for stainless steel and spring steel is similar. However, for larger deflections spring steel remains in a larger elastic region for deformations. This means that the relative stiffness does not change much and a proof of concept can be carried out using stainless steel. When results using stainless steel are accurate, changing the material to spring steel in simulations can help to rapidly determine the results for larger deflections. Now, the manufacturing plan and material for manufacturing are clear. In the next section, it is explained how the final design was produced.

7.2. Manufacturing

To conduct experiments on a prototype and verify the results from the optimizer, the structure was manufactured. The first step to manufacture the design is to laser-cut it out of a stainless steel plate by exporting the strip from figure 7.2 as a .dxf file. The next step is to use a roll bending machine to bend the laser-cut strip into the exact arc, which is shown in figure 7.3. The roll bending machine has three rollers, two rollers are used to guide the structure. One of these rollers can be manually turned by the yellow handle to guide the structure through the machine, shown in figure 7.3. The third roller is used to bend the structure. The position of this third roller can be changed manually such that the resulting curve of the bend structure changes. The third roller can also be moved by a handle to locally apply more bending. Using this machine resulted in the structure surrounding the paper shown in figure 7.3. This structure has a constant curve with two local folds to approximate the untwisted structure.
To complete the manufacturing, the curved structure is clamped in a vise exactly in the middle point. To create the twist, the endpoints are moved using pliers, shown in figure A.18. The resulting structure can be seen in figure 7.4.

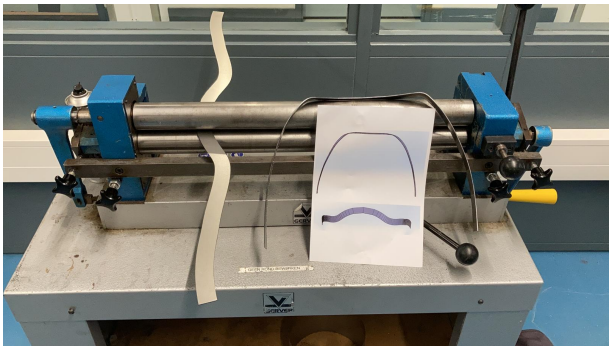

Figure 7.3: Roll bending the laser-cut strip to fabricate the untwisted configuration of the optimized beam.

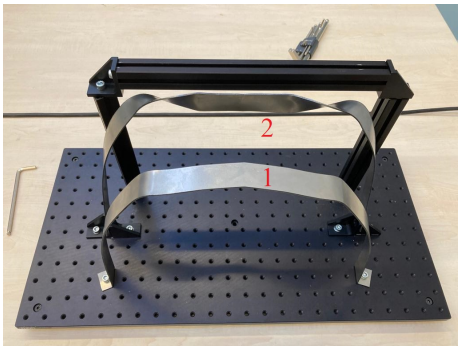

Figure 7.4: Prototype in untwisted configuration (1) and final design (2).

8

Results

To find out if the manufactured design provided satisfactory results, experimental tests were performed. The experimental results verify the results from the self-developed optimizer with the real world. The original design from the wearable robotics project is also verified using a commercial FEM software.

8.1. Simulation results

To verify the results, a commercial FEM software was used namely ANSYS Mechanical®. A static structural analysis was conducted using structural steel as a material. Solid modelling was used for both design verification with reality and comparing the optimized structure to the original design. In the next sections, simulations are provided for the comparison of the results from the beam optimizer, the results from experiments and the original design from the wearable robotics project.

8.1.1. Performance analysis

This analysis was executed to compare the original design with the optimized design. The original design consisted of 3 parts, 2 beams and a connection in between, as can be seen in figure 4.1. The beam path was dependent on different guide curves to follow the human body. The beams had multiple screw holes to adjust the support to a person's height.
For the simulation, the fixed supports were added to the middle screw hole at the endpoints of the two curved beams. The forces and moment were applied to the middle hole of the connection part in between. One important assumption that was taken, was that the three parts were perfectly connected and this was achieved using the combine function from the applied CAD modelling program. A force of 325 N in x-direction led to a directional deformation of 2.7mm in the corresponding forward bending direction of the user. A force of 325 N in y-direction led to a directional deformation of 2.6mm in corresponding lateral bending direction of the user. The applied moment of 65 Nm around the z-axis led to an angular deformation of 25 degrees. The resulting stiffness for forward bending is 120 N/mm, for lateral bending is 125 N/mm and the resulting rotational stiffness for twisting is 149 Nm/rad. The results are shown in figures 8.1, 8.2 and 8.3. The mass was retrieved from the table of geometry properties and was 0.98 kg.

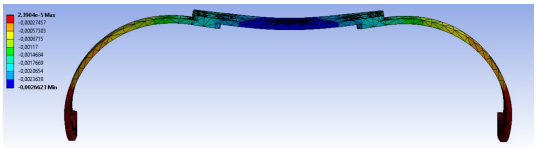

Figure 8.1: Deformation due to forward bending for an applied force of 325N.

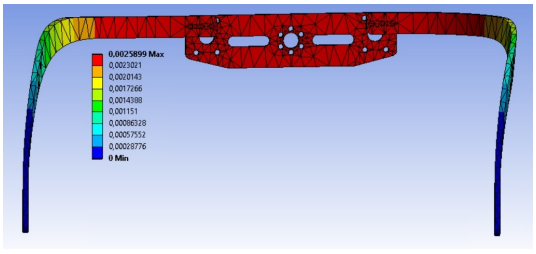

Figure 8.2: Deformation due to lateral bending for an applied force of 325N.

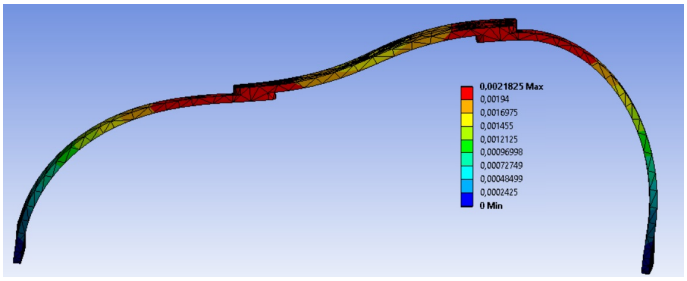

Figure 8.3: Angular deflection due to the applied torsion of 65Nm.

8.2. Experimental results

To retrieve experimental results, a test setup needed to be built. The beam made of stainless steel needed to be fixed at two locations and moved in the middle point. For the experimental test, a full-scale model was used and subjected to quasi-static loading. An initial experiment can be found in appendix A.5. Because the results were not accurate, a new test setup was made and is explained below.

To remain in the elastic limit for deformations, the structure was subjected to 51N that was a weight connected to a bolt at the middle point. How the value of 51N was determined is explained in the next subsection 8.2.1. The structure was bolted with three screws to a black plate with a rigid block to model the fixed support. The black plate could be oriented in different configurations based on the type of loading. To determine deflections, pictures were taken from the side and the distance was measured between the undeformed and deformed configuration using a measuring software. Next to the structure, a ruler was precisely positioned to obtain the correct reference scale. The resulting deflection for forward bending was 11.14mm with a corresponding stiffness of 4.58 N/mm. The setup of the experiment for forward bending is shown in figure 8.4. The resulting deflection for lateral bending was 20.16mm with a corresponding stiffness of 2.53 N/mm. The setup of the experiment for lateral bending is shown in figure 8.5. The resulting angular deflection for twisting 1.4 degrees with a corresponding rotational stiffness of 417 Nm/rad. The setup of the experiment for twisting is shown in figure 8.6.

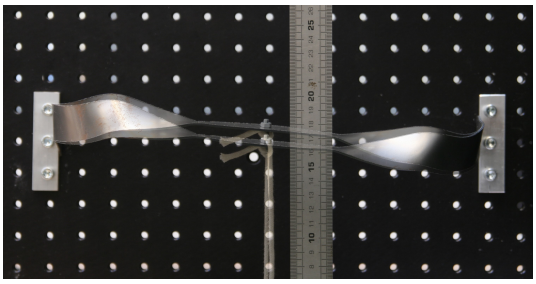

Figure 8.4: Forward bending experiment with undeflected and deflected configuration. The structure was subjected to a force of 51N.

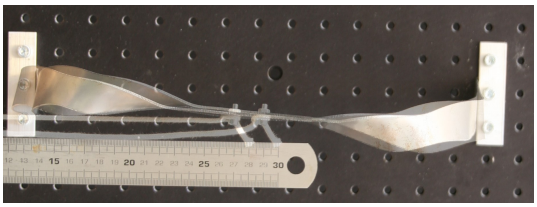

Figure 8.5: Lateral bending experiment with undeflected and deflected configuration. The structure was subjected to a force of 51N.

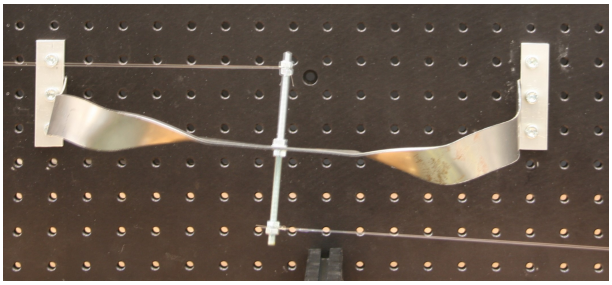

Figure 8.6: Torsional deflection with undeflected and deflected configuration. The structure was subjected to a moment of 10Nm.

8.2.1. Verification experiments

For experiments, the stainless steel prototype had to remain in the elastic region for deformations. The maximum deflections in the elastic region were calculated by applying varying forces and moments on the structure in ANSYS Mechanical® and plotting the stresses (equivalent von-Mises) throughout the structure. The next step was comparing the maximum stress with the yield limit of stainless steel. It was calculated that the maximum force within the yield limit was an applied force of 51N in lateral bending direction. This resulted in a maximum stress of 250 MPa which was found to be the yield stress for stainless steel [28]. This resulted in forward bending of 10.2mm and lateral bending of 17.5mm. This is shown in figures 8.7 and 8.8. The resulting stiffness for forward bending is 5 N/mm and for lateral bending is 2.9 N/mm. The angular deformation for applied torsion of 10 Nm was 4.7 degrees. This is shown in figure 8.9. The resulting rotational stiffness for twisting is 124 Nm/rad.

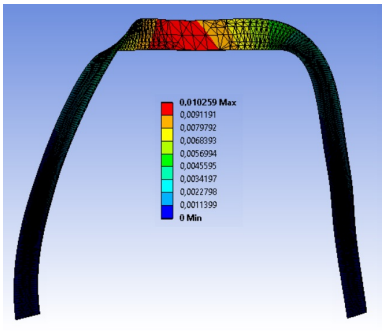

Figure 8.7: Forward elastic bending deflection for an applied force of 51N measured using ANSYS Mechanical®.

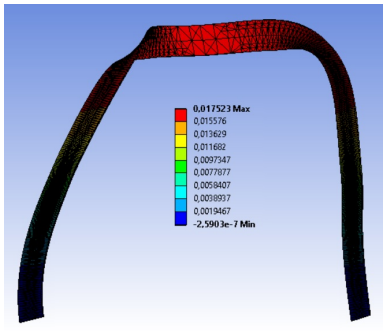

Figure 8.8: Lateral elastic bending deflection for an applied force of 51N measured using ANSYS Mechanical®.

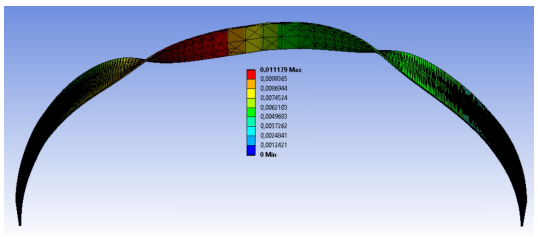

Figure 8.9: Topview of the structure giving total deformation for an applied moment of 10Nm for torsional deflection. This was measured using ANSYS Mechanical®.

8.3. Overview of the results

An overview of the resulting stiffnesses that were obtained for the bending simulations using force and deflection specifications from the requirements is shown in table 8.1. An overview of resulting stiffnesses for experiments using scaled-down forces and deflections is shown in table 8.2.

	Forward bending	Lateral bending	Twisting
Optimizer	**32.5 N/mm**	5.4 N/mm	155 Nm/rad
ANSYS®	**7.93 N/mm**	4.71 N/mm	120 Nm/rad
Original	120 N/mm	125 N/mm	149 Nm/rad

Table 8.1: Overview of optimization and simulation results for an applied force of 325 N and applied moment of 65 Nm. The average stiffness is provided in forward bending, lateral bending and twisting. The results generated from optimization (Optimizer) are verified in a commercial FEM software (ANSYS®) and the results for simulating the original support from the wearable robotics project in the commercial FEM software (Original). Highlighted is the significant difference between the results from optimization and ANSYS® for forward bending.

	Forward bending	Lateral bending	Twisting
ANSYS®	5 N/mm	2.9 N/mm	**124 Nm/rad**
Experiment	4.58 N/mm	2.53 N/mm	**417 Nm/rad**

Table 8.2: Overview of simulation and experimental results for an applied force of 51 N and applied moment of 10 Nm. The average stiffness is provided in forward bending, lateral bending and twisting. In the elastic region, the results from simulating the final beam design using a commercial FEM software (ANSYS®) are compared with experimental results (Experiment). Highlighted is the significant difference between the results from ANSYS® and experiments for twisting.

9 Discussion

Comparing the results from optimization with a commercial FEM software resulted in satisfying stiffnesses in lateral bending direction and twisting. However, a significant difference was found for forward bending. The obtained stiffness from the optimizer was 32.5 N/mm but the obtained stiffness from the commercial FEM software was 7.93 N/mm. This means that the beam optimizer did not provide comparable results that are expected from FEM simulations. The expected reason for this was that the resulting structure from the optimizer was too thin. To be more specific, the optimized beam had a cross-section ratio of 1 to 18. Thin structures subjected to large deflections are not modelled well by the employed beam model. This model has limitations, namely cross-sectional deformations such as warping and in-plane deformations are suppressed. This is needed for modelling thin structures subjected to large deformations. It shows that it can be difficult to use optimization when it is unknown what the solution will be approximately or proper constraints should be applied to the cross-section ratio. When the results from optimization are outside the region in which it can provide satisfying results, the outcome will simply not be satisfying. So for future work, 2D shell modelling can be considered to improve results as it is expected that this modelling technique can better model thin structures subjected to large deformations.

To better substantiate this idea, the stiffness behaviour for forward bending was visualized for large deflections using the optimizer based on beam modelling and comparing this with a commercial FEM software using solid modelling. This investigation is described in appendix A.6. In this investigation was found that for forward bending using solid modelling, the vertical parts of the optimized structure were subjected to torsional deformation. These vertical parts are defined in appendix A.6. This torsional deformation was also noticed in experiments. For forward bending using beam modelling, the vertical parts of the optimized structure did not result in torsional deformation. This resulted in a much higher forward bending stiffness in the optimizer. This is similar stiffness behaviour as described in chapter 5.1, where a coupled motion of twisting and forward bending leads to a decreased forward bending stiffness for thin leaf flexures. It is expected that 2D shell modelling will improve results because this technique can model the angular deformations in the vertical parts better as in-plane deformations are not suppressed.

Comparing the results from FEM simulations with experiments, the forward bending stiffness and lateral bending stiffness are comparable. However, a significant difference was found for twisting. The main reason for this was that the applied moment on the structure did not lead to a perfect rotation but to a combination of bending and rotation in the experiment. Since the rotations were quite small, this extrapolates the difference between these results.

Comparing the final beam design to the original beam design shows improvements. For the same loadings and material, the final beam design has 27 times more lateral flexibility, 1.25 times more torsional flexibility and a design that is four times lighter in comparison to the original design. The original relative stiffness of 1 to 1 for forward relative to lateral bending improved to 2 to 1.

To improve the final result, i.e. the optimized beam, an important aspect needs to be taken into account. The kinetostatic behaviour that this compliant hip-back support should be able to handle is rather complex. This is because the structure is subjected to relatively large forces but also to relatively large deflections. A structure that is subjected to relatively large forces, generally leads to a thicker structure. Whereas a structure that undergoes large deflections, generally results in a thinner structure. Finding solutions to work around this will improve results.

One idea to improve results was to reinforce the horizontal middle part of the optimized beam. The elaboration of this concept is further described in appendix A.7. In this elaboration, it is explained that the relative stiffness for forward to lateral bending increased but that the compliance in twisting direction decreased. Therefore, this is not an ideal solution.

Another idea to improve the beam design was based on the FACT concept from section 5.1.1. This was to divide the support in a compliant and rigid part. For the rigid part, a stiff planar beam needs to be designed. This can be made using a different cross-section and material, e.g. a composite material, that is relatively lightweight and stiff. The compliant part can be developed as a simple flexure design problem. The material for this part should have a relatively high yield strength to allow for large deformations. This idea might lead to a heavier structure as not the complete structure is included in the compliance behaviour. This idea can also be extended using optimization. That is to optimize a structure for one rigid part and one compliant part. This idea can also be included for future work.

10

Conclusion

For the development of a compliant hip-back support, this work starts with the state of the art of relevant hip-back supports and research projects. Next, the characterization methods of compliant mechanisms were reviewed for inspiration, to come up with a suitable design method for developing a compliant structure for a hip-back support. By tuning stiffness of the structure in distinct directions, a conventional synthesis method for compliant mechanisms could be applied, namely the Freedom and Constraint Topologies method. This was used to come up with a preliminary design. This design was extended to improve stiffness behaviour for coupled motions and four promising high-level designs were worked out that could handle this rather complex kinetostatic task. To generate an even more satisfying solution, optimization of the beam shape was applied to handle the complex kinetostatic task and to develop a lightweight structure. To generate a design, a self-developed optimizer using beam modelling was extended and applied. The extensions were to optimize a double-clamped beam that was loaded in the middle point and optimizing for angular deformations as a set objective function. This extended optimizer generated the final design which was a thin rectangular-shaped beam with three-dimensional curves. Different manufacturing methods were evaluated to fabricate this design and the optimized shape was eventually produced by laser-cutting a strip which was extracted from flattening of the spatial shape. Then, the prototype was produced by roll bending the strip into a curved beam and manually applying a twist in the middle point to create a satisfying approximation of the final design. Experimental tests for forward bending, lateral bending and twisting were conducted on the prototype. The results were, for the same loadings and material, 27 times more lateral flexibility, 1.25 times more torsional flexibility and a design that is four times lighter in comparison to the original design. The original relative stiffness of 1 to 1 for forward relative to lateral bending improved to 2 to 1. One of the main findings was that using 1D beam modelling to model thin structures that are subjected to large deflections is less suitable. To better model these thin structures that are subjected to large deformations, one can extend the optimizer to use 2D shell modelling. This can be considered for future work and is expected to improve results.

Another concept that could be further investigated to improve results is the FACT concept from section 5.1.1. This concept divides the three-dimensional complex kinetostatic problem into a compliant leaf flexure design and a planar rigid design. This might increase the weight of the design but simplifies the compliance problem to a more simple flexure design. Further investigation of combining different types of cross-sections for the rigid part and materials is expected to provide improved results for this kinetostatic problem. This idea can also be extended using optimization. That is to optimize the shape of a structure for one rigid part and one compliant part. This idea can also be considered for future work.

Bibliography

[1] Griffith, L. E., Shannon, H. S., Wells, R. P., Walter, S. D., Cole, D. C., Côté, P., Frank, J., Hogg-Johnson, S., & Langlois, L. E. (2012). Individual participant data meta-analysis of mechanical workplace risk factors and low back pain. American journal of public health, 102(2), 309–318. https://doi.org/10.2105/AJPH.2011.300343

[2] Beeck, R. O., & Hermans, V. (2000). Research on Work-related Low Back Disorders. Institute for Occupational Safety and Health.

[3] Eurofound (2012). Fifth European Working Conditions Survey. Technical report, Publications Office of the European Union.

[4] Näf, M.B., Koopman, A.S., Baltrusch, S., Rodriguez-Guerrero, C., Vanderborght, B. and Lefeber, D. (2018) Passive Back Support Exoskeleton Improves Range of Motion Using Flexible Beams. Front. Rob. AI, 5, p. 72

[5] Laevo Exoskeleton. (n.d). LAEVO EXOSKELTON A Complete Consumer Guide. Retrieved from: http://www.laevo-exoskeleton.com/

[6] Wesslén, J. (2018). Exoskeleton exploration : Research, development, and applicability of industrial exoskeletons in the automotive industry (Dissertation). Retrieved from http://urn.kb.se/resolve?urn=urn:nbn:se:hj:diva-40093

[7] Looze de, M.P., Bosch, T., Krause, F., Stadler and K.S., O'Sullivan, L.W. (2015) Exoskeletons for industrial application and their potential effects on physical work load. Ergonomics. http://dx.doi.org/10.1080/00140139.2015.1081988.

[8] A. Voilqué, J. Masood, J. Fauroux, L. Sabourin and O. Guezet, "Industrial Exoskeleton Technology: Classification, Structural Analysis, and Structural Complexity Indicator," 2019 Wearable Robotics Association Conference (WearRAcon), Scottsdale, AZ, USA, 2019, pp. 13-20, doi: 10.1109/WEARRACON.2019.8719395.

[9] Brent L. Ulrey, Fadi A. Fathallah, Effect of a personal weight transfer device on muscle activities and joint flexions in the stooped posture, Journal of Electromyography and Kinesiology, Volume 23, Issue 1, 2013, Pages 195-205, ISSN 1050-6411, https://doi.org/10.1016/j.jelekin.2012.08.014.

[10] M. M. Holscher, B. B. Maat, R. Huitema, and B. M. Wisse, "Wearable support structure for at least partly relieving a human body during leaning or bending over," Patent WO2 016 148 566A1, 2016

[11] Maurice, P., Čamernik, J., Gorjan, D., Schirrmeister, B., Bornmann, J., Tagliapietra, L., Latella, C., Pucci, D., Fritzsche, L., Ivaldi, S. and Babic, J. (2019). Objective and Subjective Effects of a Passive Exoskeleton on Overhead Work. IEEE Transactions on Neural Systems and Rehabilitation Engineering. PP. 1-1. 10.1109/TNSRE.2019.2945368.

[12] Tsuzura, M., Nakakuki, T., & Misaki, D. (2013). A mechanism design of waist power assist suit for a caregiver by using torsion springs. 2013 13th International Conference on Control, Automation and Systems (ICCAS 2013), 866-868.

[13] H. Kazerooni, E. Hacker, L. Chen, W. Tung, N. Poon, and T. Yangyuenthanasan, "Trunk supporting exoskeleton and method of use," Patent WO2 017 086 946A1, 2017.

[14] Alemi, M., Geissinger, J., Simon, A., Chang, S. and Asbeck, A. (2019). A Passive Exoskeleton Reduces Peak and Mean EMG During Symmetric and Asymmetric Lifting. Journal of Electromyography and Kinesiology. 47. 10.1016/j.jelekin.2019.05.003.

[15] https://www.wearablerobotics.nl/

[16] Visual Centers of Gravity. (2013, 21 december). The VisionHelp Blog. https://visionhelp.wordpress.com/2013/12/20/visual-centers-of-gravity/

[17] Human sized of standing person. Obtained via http://dined.io.tudelft.nl/dined/full

[18] Cratsborn, T., Amoozandeh Nobaveh, A., Radaelli, G., Herder, J.L. (2020) Investigation in characterization methods of compliant machanisms.

[19] Hibbeler, R. C. (2003). Mechanics of materials. Upper Saddle River, N.J: Pearson Education.

[20] Staats, L. (2020) Review on methods of controllable stiffness for structures.

[21] Veritasium. (2020, December 15). Engineering with Origami [Video file]. Retrieved from https://www.youtube.com/watch?app=desktop&v=ThwuT3_AG6w

[22] McEvoy, M. A., Farrow, N., Correll, N. (2013). Robotic materials with controllable stiffness. Proceedings of the 19th International Conference on Composite Materials (ICCM).

[23] Xie, X., Qiu, L., Yang, D. (2020). Analysis of a novel variable stiffness filleted leaf hinge. Mechanism and Machine Theory, vol. 144, p. 103673.

[24] Lachenal, X., Daynes, S., & Weaver, P. M. (2014). A non-linear stiffness composite twisting I-beam. Journal of Intelligent Material Systems and Structures, 25(6), 744–754. https://doi.org/10.1177/1045389X13502853

[25] Amoozandeh Nobaveh, A., Radaelli, G., Herder, J.L. (2020) Asymmetric Spatial Beams with Symmetric Kinetostatic Behaviour.

[26] Hoschek, J., Lasser, D. (1993). Fundamentals of computer-aided geometric design. A.K. Peters.

[27] Battini, J.M. (2002). Co-rotational beam elements. Ph.D. thesis, Royal Institute of Technology, Stockholm, Sweden.

[28] Engineering ToolBox, (2003). Young's Modulus - Tensile and Yield Strength for common Materials. [online] Available at: https://www.engineeringtoolbox.com/young-modulus-d_417.html [Accessed at 3.2.2021].

[29] Chatti, S., Hermes, M., Tekkaya, A. E., & Kleiner, M. (2010). The new TSS bending process: 3D bending of profiles with arbitrary cross-sections. CIRP Annals, 59(1), 315–318. https://doi.org/10.1016/j.cirp.2010.03.017

[30] Wikipedia contributors. (2021, 1 februari). Spring steel. Wikipedia. https://en.wikipedia.org/wiki/Spring_steel

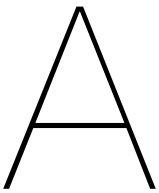

Appendix

A.1. State of the art

This section provides images of four passive mechanical exoskeletons that use rigid beams in combination with springs. The four exoskeletons are the Bending non-demand return, Ottobock Paexo back, Power assist suit (PAS) and SuitX BackX.

Figure A.1: Bending non-demand return (BNDR)

Figure A.2: Ottobock Paexo back

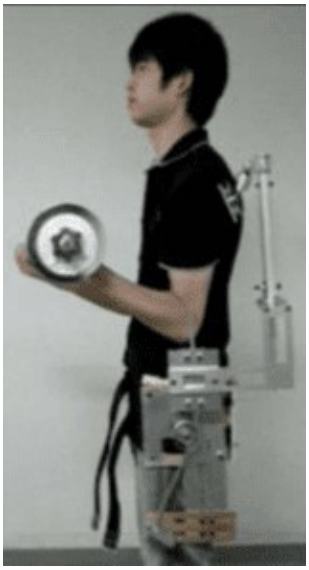

Figure A.3: Power assist suit (PAS)

Figure A.4: SuitX BackX

A.2. Verification FACT Design

Verification of the leaf flexure design is done in a commercial FEM software, i.e. ANSYS Mechanical®. A static structural analysis was conducted for large deflections and shown in figures A.5, A.6 and A.7. The result for bending was 5% higher than expected but this was close enough to the calculated value. The result for lateral bending was 13% lower than expected and this inaccuracy is expected for large deformations. This is because the forget-me-not formulas are most accurate for small deflections in the elastic deformation region. The result for torsion was 80 degrees and this was 267% larger than expected.
It is important to note that these deformations are in the plastic region for structural steel. That means that the stresses in the material exceeded the yield stress. The highest stress measured in the material for the three applied load cases was 2695 MPa which is relatively large. Lowering the forces to 110N, lowering the moments to 22 Nm and using 301 spring-tempered stainless steel as the material will let the structure remain within the elastic limit. Then, the equivalent stress is comparable to the yield stress of this specific spring steel, i.e. 1014 MPa [30].

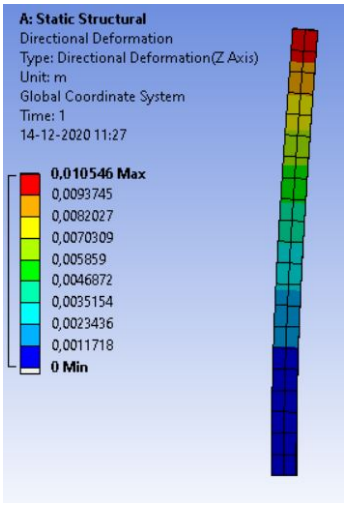

Figure A.5: Bending deformation for an applied force of 325N.

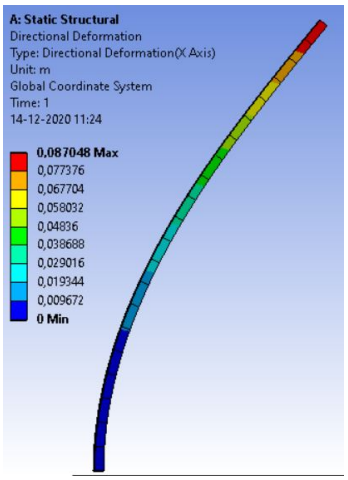

Figure A.6: Lateral bending deformation for an applied force of 325N.

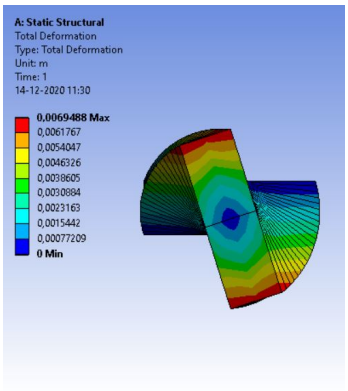

Figure A.7: Deformation in twisting direction for an applied moment of 65Nm.

A.2.1. Combination of deflections full

Another investigation was done on the combination of deflections using maximum force and moment combinations in two out of the three directions, using structural steel as the material.
In figure A.8, the deflection is shown for a combination of bending and lateral bending. Two forces of 325N are applied and provide a result that looks like the superposition of A.5 and A.6. This means that there does not happen anything that was not expected.
In figure A.9, the combination of bending and torsion is visualized. The applied force is 325N and the applied moment is 65Nm. The results do not look like a superposition of bending and torsion. After the flexure is twisted, the bending stiffness decreases dramatically. This influence of torsion on bending stiffness needs to be taken into account when designing a leaf flexure for coupled motions.
In figure A.10, a combination of lateral bending and torsion is applied. This resulted in a similar outcome as is expected from the superposition of A.6 and A.7.

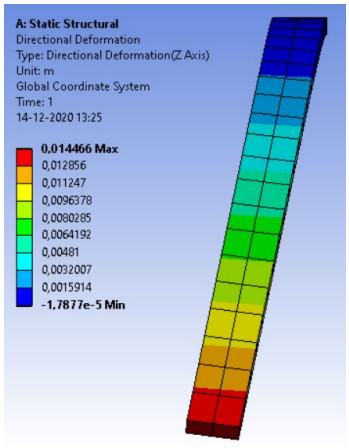

Figure A.8: Deformation shown for a combination of bending and lateral bending for two directionally applied forces of 325N.

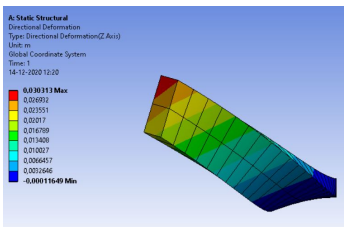

Figure A.9: Deformation shown for a combination of bending and torsion for an applied force of 325N and an applied moment of 65Nm.

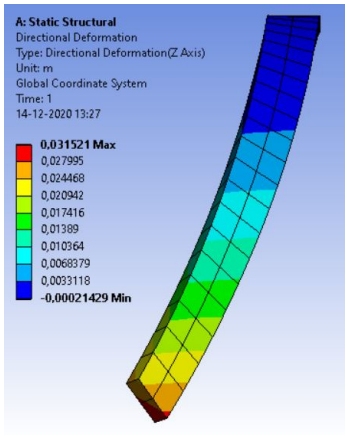

Figure A.10: Deformation shown for a combination of lateral bending and torsion for an applied force of 325N and an applied moment of 65Nm.

A.2.2. Combination of deflections at 20%

As the combination of forces and moments at 100% in two directions is not expected in practice, a combination of 100% and 20% is investigated, using structural steel as the material. This is done to investigate if a lower applied torque in twisting direction still results in a relatively large decrease in bending stiffness for a combination of deflections. In the simulations, one direction is subjected to the full force of 325N or a moment of 65Nm. The other direction is subjected to 20% of the 325N force or 20% of the 65Nm moment, i.e. 65N or 13Nm. In figure A.11, lateral bending in combination with bending is visualized. In figure A.12, a combination of bending and lateral bending is shown. Figure A.13, shows the combination of bending and torsion. Lastly, figure A.14 shows the combination of lateral bending and torsion. A conclusion can be drawn that for thick leaf flexures subjected to relatively small angular deformations due to the applied torsion, stiffness does not decrease much in the bending direction. Comparing the results from A.5 and A.13 show a 10% decrease in stiffness as the deflection increases from 10.5 mm to 11.7 mm. Other results were also comparable as is expected from the superposition of two individual deflections.

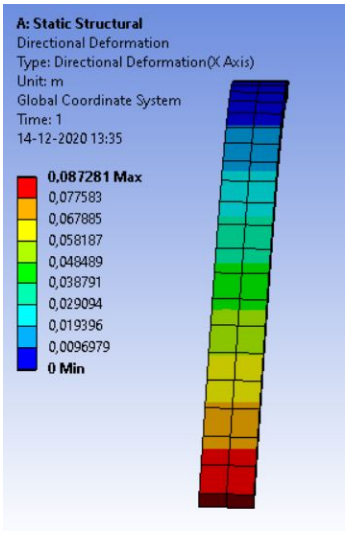

Figure A.11: A combination of lateral bending with an applied force of 325N and forward bending with an applied force of 65N.

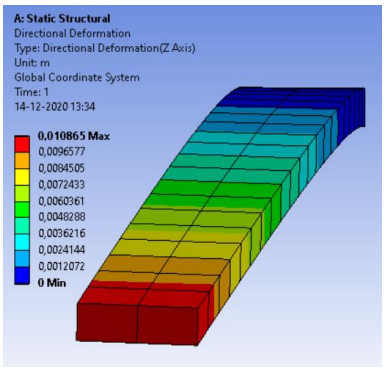

Figure A.12: A combination of forward bending with an applied force of 325N and lateral bending with an applied force of 65N.

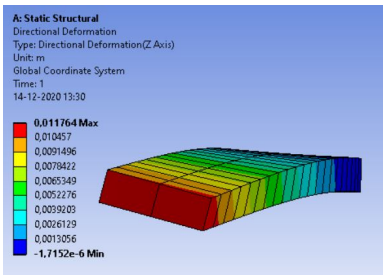

Figure A.13: A combination of forward bending with an applied force of 325N and twisting with an applied moment of 13Nm.

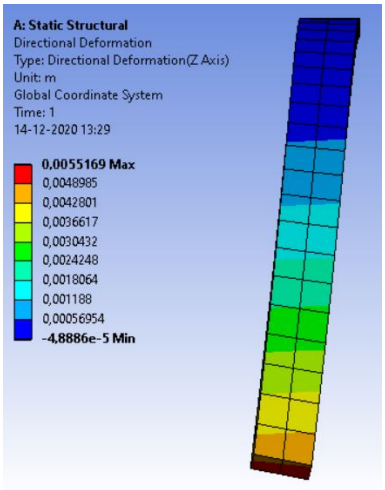

Figure A.14: A combination of lateral bending with an applied force of 325N and twisting with an applied moment of 13Nm.

A.3. Manufacturing Methods

To understand how to manufacture the resulting optimized design, a variety of manufacturing specialists were contacted. They made clear that this 3D complex shape that resulted from the optimizer was not simple to fabricate. Therefore, different manufacturing methods were investigated. The most promising methods are explained below.

3D printing

A promising method is 3D printing though developments on this method are needed. 3D printing is a good production method for low batch size and can create complex 3D shapes. An example of 3D printing is electron beam melting which is used to manufacture for example titanium designs. The issue with 3D printing is that fatigue life is not great due to many imperfections that remain after the part is 3D printed. However, for a prototype, it might suffice for small deflections. This method is not selected because the costs for manufacturing are outside the scope of this thesis.

Casting

For casting, molten metal is poured into a mould to achieve a specific form. CNC milling a mould is often used for casting and this can achieve an exact shape. This method is very precise but often cast structures need to be heat treated because the cast material is relatively brittle. Therefore, these cast structures do not allow for cycles of large deflections. The same reason applied, as to metal 3D printing, that fatigue life is not expected to be satisfying. This method is more suitable for large batch size production due to the relatively high start-off costs for producing a mould. This method is not selected because the costs for the production of a mould are outside the scope of this thesis.

Bending

To verify if the structure would not break when it is bent from a straight strip to the curved strip shown in figure 7.2, stresses were measured by simulations. In figure 7.2, the distance was measured between one endpoint and the middle point in the vertical direction using the Measure tool in SolidWorks®. The distance was 29.7mm and is used as directional deformation. In ANSYS Mechanical®, a straight cantilever beam with the same cross-sectional dimensions was deformed using the obtained directional deformation and stresses were measured. An important assumption was that the stresses in this simplified configuration could approximate the stresses that arise when bending the complete structure using a bending machine. For an input deformation of 29.7mm, the corresponding maximum equivalent von-Mises stress was 1680 MPa and is shown in figure A.15. This is a relatively large stress but multiple steel types can handle these large stresses. An idea to decrease the maximum stress is to apply constraints to the maximum bending curvatures of the spine shape of the optimized beam.

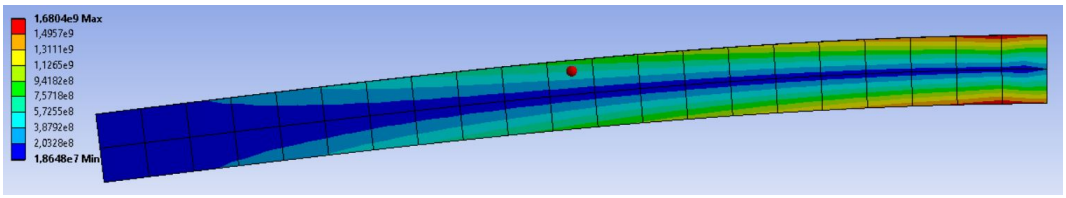

Figure A.15: Simplification to calculate the maximum stress that arises when bending a straight strip into the curved strip shown in figure 7.2, using a cantilever beam and specified directional deformation.

To produce a prototype of the final design, a novel bending machine can be used that was developed by the TU Dortmund. This manufacturing device is called the Torque Superposed Spatial (TSS) bending machine [29] which is shown in figure A.16. The machine works by having one static and one moving plane with 2 translations and 1 rotation. This can create profiles with three-dimensional bending contours. The input structure that will be bend, needs to have a square cross-section. Filling up sections such as H, Z, C beams to a square cross-section allows for multiple cross-sections to be curved in complex 3D shapes. Since the costs for using this device were outside of the scope for this thesis, this method was not selected.

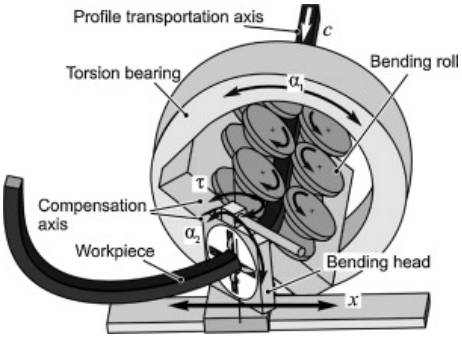

Figure A.16: Principle of the Torque Superposed Spatial (TSS) bending process [29].

Roll bending

In metalworking, rolling is a metal forming process in which a structure is passed through multiple rolls to change the thickness or curvature of a structure. Rolling generated multiple ideas, one was to use the double triple roll bending machine where the middle plane could twist. However, this would not result in the desired shape as the exit plane was not able to apply a twist to the beam. Another idea was to use a twisting roller but there were no machines available with this ability. Using a standard roll bending machine could achieve relatively accurate curvatures along the beam in one direction. This idea could partly solve the manufacturing from the curved strip to get an approximation of the optimized beam shape.

Final method

The final method, to produce the optimized beam, is to use roll bending to bend the beam into the right arc. This method can be used to create a precisely curved beam but a twist is needed after this step to create the complete 3D shape. This twist can be applied using pliers when the structure is clamped in a vise. This method approximates the shape of the optimized beam.

A.4. Spring steel test

To determine if it is possible to use spring steel for manufacturing, experiments were done on multiple spring steel strips. However, first is explained how to create the final design from the beam optimizer using spring steel.
There are two ways to produce this design, one is to bend and twist a structural steel structure into the right shape and use heat treatment with quenching to create the right material properties comparable to spring steel. The second way is to bend spring steel but this material can be relatively brittle and has a lot of spring back which makes the production quite complex.
To investigate the possibilities of using spring steel, an experiment to bend and twist spring steel was executed to better understand the stiffness behaviour of spring steel. As can be seen from figure A.17, roll bending spring steel resulted in more curvature as the thickness increased. Twisting also led to promising results but at a lower thickness, the material broke for large deformation, which is shown in figure A.18.
The experiment was successful and this means that it is possible to make a prototype out of spring steel using roll bending and pliers. For a proof of concept, it was not needed to develop a prototype using expensive spring steel. Using stainless steel can give an indication of relative directional stiffness for a proof of concept. This is because steel is a linear material.

Figure A.17: Spring steel bending test using strips with thicknesses of 0.5mm, 0.75mm and 1.0mm. Increasing the thickness leads to an increased curvature of the strip.

Figure A.18: Twisting spring steel strip of thickness 0.5mm, 0.75mm and 1.0mm. The results show that the strip with 0.5mm thickness broke after a twist was applied. The used pliers and glove for this experiment are also shown.

A.5. First experiment

The first experiment that was conducted on the manufactured beam is explained below. The test setup and results from this experiment are provided. After this, the reason for error between the simulations and experiments is explained.

A.5.1. Setup of the first experiment

For the forward bending experiment a bridge with a ruler was connected over the structure. The bridge was aligned with the middle point to measure the exact deflection at this point. The structure was bolted to the black plate and subjected to a loading of 51N to remain in the elastic region. The deflections were measured using observations and pictures. The setups are shown in figures A.19 and A.20.
The results for the forward bending test lead to a deflection of 15mm. The results for lateral bending are 17mm deformation. These results are shown in figure A.21 and A.22.

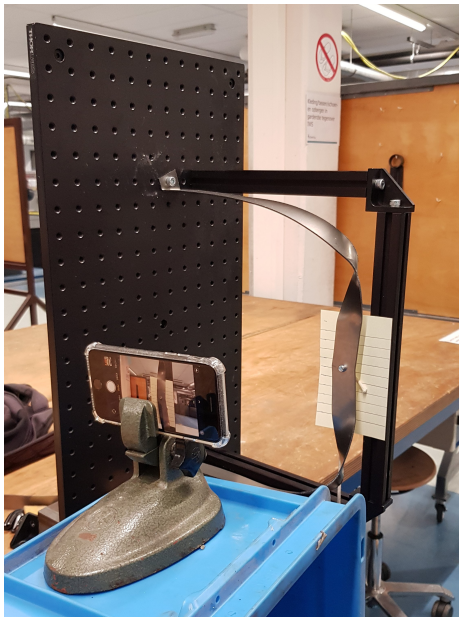

Figure A.19: Setup lateral bending experiment

Figure A.20: Setup forward bending experiment

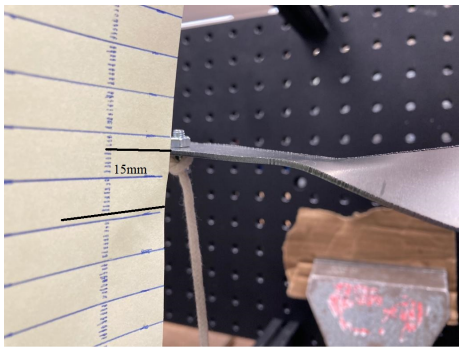

Figure A.21: Forward bending experiment

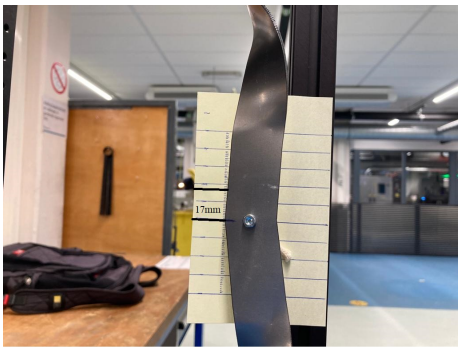

Figure A.22: Lateral bending experiment

A.5.2. Error in the first experiment

In the first experimental test setup for forward bending, the results were different from the results using a commercially available FEM software. The expected 8mm deflection in forward bending direction was in reality 15mm. Comparing the pictures that were taken from the experiment, it was noticed that the bolted endpoints were not an ideal fixed support for forward bending. The loading in this configuration led to torsion on the endpoints connected to the black supporting plate. This led to an

angular deformation of the fixed support that was causing the disturbance in the results. One degree of angular deformation already leads to a displacement of 3.5mm at the middle point. The angular deformation is shown in figures A.23 and A.24 by a red line. To improve this test setup, for the new tests, a steel block was bolted at three points over the bent flanges at the endpoints. This better models the fixed supports.

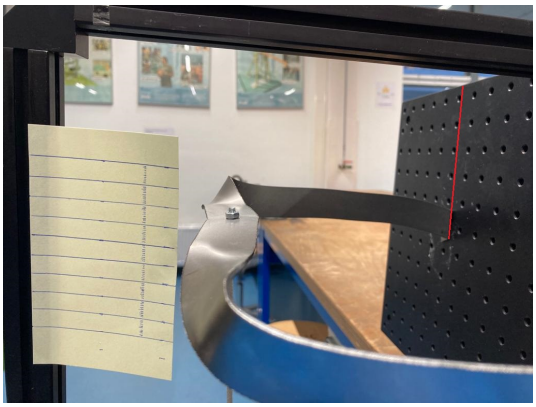

Figure A.23: Experiment forward bending with no applied load, highlighting the angular deformation of the fixed support.

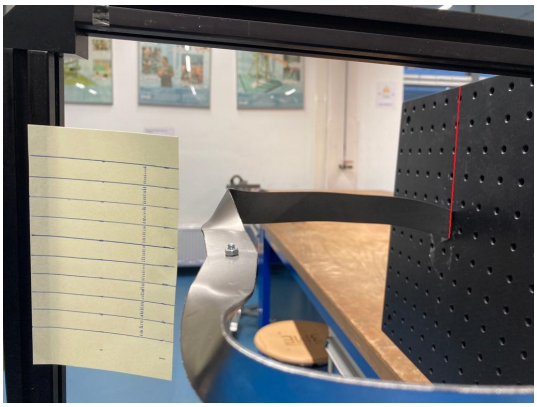

Figure A.24: Experiment forward bending with applied load, highlighting the angular deformation of the fixed support.

A.6. Comparison Optimizer and ANSYS® deformation for forward bending

The goal of this section was to visualize the difference between the optimizer and the commercial FEM software for a forward bending displacement of 41mm. The optimizer had a larger forward bending stiffness and the applied force was increased until the structure reached the deflection of 41mm. The figures below show that the most deformation in the optimizer comes from the horizontal middle part. This horizontal middle part is defined by the blue line in figure A.25. The most deformation from the FEM software comes from the angular deflection of the vertical parts of the beam. These vertical parts are defined by the two orange lines in figure A.25. When the vertical parts of the beam twist, the angular deformation deflects the middle point of the beam.

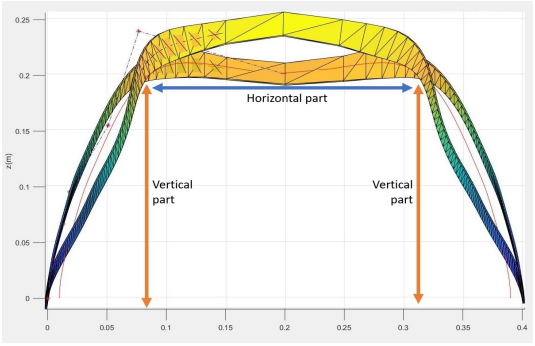

Figure A.25: Front view of the results from optimization with undeformed configuration (orange) and deformed configuration (yellow). The vertical parts defined in the text are indicated by two orange lines. The defined horizontal part is indicated with a blue line.

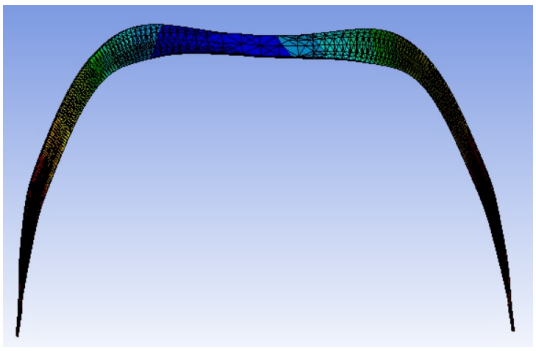

Figure A.26: Front view of results from FEM analysis showing the deformed configuration.

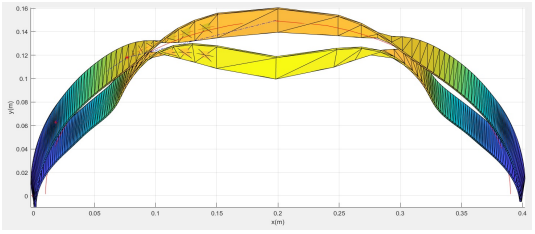

Figure A.27: Top view of the results from optimization with undeformed configuration (orange) and deformed configuration (yellow).

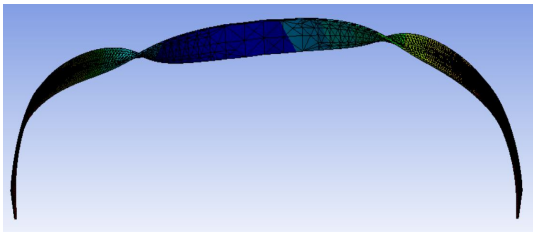

Figure A.28: Top view of results from FEM analysis showing the deformed configuration.

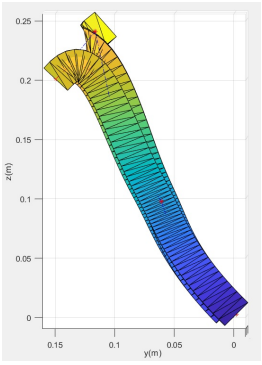

Figure A.29: Side view of the results from optimization with undeformed configuration (orange) and deformed configuration (yellow).

Figure A.30: Side view of results from FEM analysis showing the deformed configuration.

A.7. Reinforced structure

To research if reinforcing the middle part of the structure improves the stiffness behaviour of the final beam design, the shape was thickened to 4.5 mm at two random but symmetrical locations. Simulations by applying a force of 325N led to a forward bending deflection of 25 mm and a lateral bending deflection of 68 mm. Applying a moment of 65Nm led to an angular deformation of 23 degrees in the twisting direction. The resulting stiffness for forward bending is 13 N/mm and for lateral bending is 4.8 N/mm. The resulting rotational stiffness for twisting is 162 Nm/rad. These results can be found in figures A.31, A.32 and A.33. From the original stiffness for forward bending of 7.93 N/mm, lateral bending of 4.71 N/mm and rotational stiffness for twisting of 120 Nm/rad. It can be concluded that the relative stiffness between forward and lateral bending improves but the stiffness for twisting increases. This means that reinforcing the middle part is not an ideal solution.

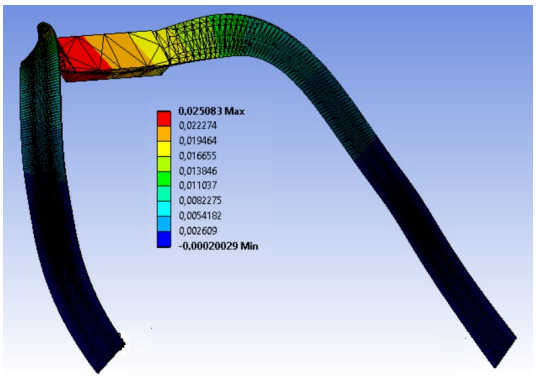

Figure A.31: Final design reinforced and subjected to a force of 325N in forward bending direction.

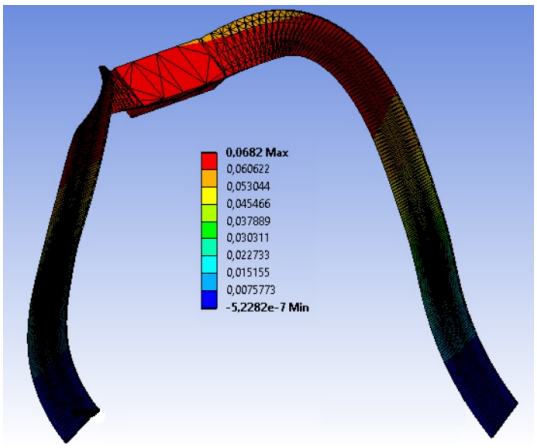

Figure A.32: Final design reinforced and subjected to a force of 325N in lateral bending direction.

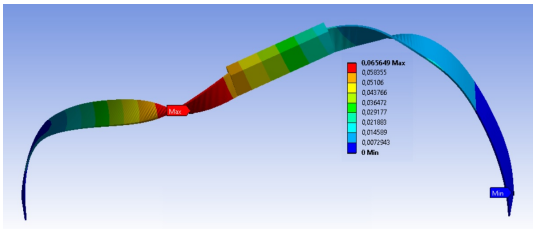

Figure A.33: Final design reinforced and subjected to a moment of 65Nm in twisting direction.

A.8. ShapeOptimizerWrist MATLAB® code

```
close all;
clear
clc
sp = 7;

%Starting point
ys
    =[0.0341048116183500,0.0533655621565439,0.0626617531936104,0.0999328206361504,0.118003

zs
    =[0.0334088134124956,0.0661823288485580,0.0950301759947651,0.154176256495563,0.2389218

CSD=[0.0274657297665602,0.0015,0,0,0];
Ori
    =[9.01003696872009,3.82163757398409,0.958493553875226,0.129809773305134,0.059544513638

x0 = [ys; zs; CSD; Ori];

%Bounds
lb = [0.001*ones(1,sp-2)     ; .9*zs   ; .015    .0005    0   0    0 ; -180 -180
     -180 -180 -180];
ub = [0.149*ones(1,sp-2)     ; 1.1*zs  ; .04    .002     0    0     0 ;  180
    180   180   180   180   180];

A = [];
b = [];
Aeq = [];
beq = [];
nonlcon=[];

%Multistart
ms = MultiStart('Display','iter')
options=optimset('Algorithm','interior-point','GradObj','off','Hessian','
    off','tolX',1e-4,'TolFun',1e-5,'MaxIter',25,'MaxFunEvals',10000,'
    PlotFcns',@optimplotfval);
problem = createOptimProblem('fmincon','x0',x0,'lb',lb,'ub',ub,'Aeq',[],'
    beq',[],'nonlcon',nonlcon,'objective',@ShapeOptmultiWrist,'options',
    options);
[dims, Objbest,exitflag,output,solutions] = run(ms,problem,5)
save('optimization_results')

%Settings
par.nTimestep    = 30;
par.nIter        = 50;
par.conv         = 1e-8;
par.plots        = 'on';
nbeam            = 500;

%Results
dims
    =[0.0289162110615655,0.0452251330904591,0.0576096074393172,0.103294064413317,0.1417936


%% Model
```

```
% generation of coordinates and connectivities
xs = zeros(sp-2,1);
X=zeros(sp,3);
X(sp,1)= .2;
X(sp,2)= .15;
X(sp,3)= .2;

for q=1:sp-2
func = @(x) (2.25*(x-.2)^2)+(4*dims(1,q)^2)-0.09; % dims(1,q) = ys
x0 = .1; % starting point
xs (q,1) = abs(fzero(func,x0));
end

for m=2:sp-1
X(m,1)=xs(m-1,1);
X(m,2)=dims(1,m-1);
X(m,3)=dims(2,m-1);
end

m_beams.X=zeros(2*nbeam-1,6);
X=X';
mainCS=linspace(0,1,sp);
knots=[0 0 0 0 0 .455 .545 1 1 1 1 1];

Nurbs = nrbmak([mainCS(1,:);X(2,:)],knots);
Yi = nrbeval(Nurbs,linspace(0,1,(nbeam)));
m_beams.X(1:nbeam,2)=Yi(2,:)';
Nurbs = nrbmak([mainCS(1,:);X(3,:)],knots);
Zi = nrbeval(Nurbs,linspace(0,1,(nbeam)));
m_beams.X(1:nbeam,3)=Zi(2,:)';
for s=2:nbeam-1
func = @(x) (2.25*(x-.2)^2)+(4*m_beams.X(s,2)^2)-0.09;
x0 = .1; % starting point
m_beams.X(s,1)=abs(fzero(func,x0));
end
m_beams.X(nbeam,1)=.2;

%% Undeformed Double beam
m_beams.X(nbeam+1:2*nbeam-1,1)=.4-flip(m_beams.X(1:nbeam-1,1));
m_beams.X(nbeam+1:2*nbeam-1,2)=flip(m_beams.X(1:nbeam-1,2));
m_beams.X(nbeam+1:2*nbeam-1,3)=flip(m_beams.X(1:nbeam-1,3));


for j=1:2*nbeam-1-1
m_beams.elementNodes(j,1)=j;
m_beams.elementNodes(j,2)=j+1;
end
m_beams.numberNodes         = size(m_beams.X,1);
m_beams.numberElements      = size(m_beams.elementNodes,1);
m_beams.eqn                 = 6*m_beams.numberNodes;
m_beams.x                   = reshape(m_beams.X',m_beams.eqn,1) ;

%Spring steel
    m_beams.E           = 190e9 * ones(1,m_beams.numberElements);
    m_beams.G           = 72e9 * ones(1,m_beams.numberElements);

```

```
97  % Unisection H profile
98  CSD = dims(3,:)';
99  H = CSD(1) * ones(1,m_beams.numberElements);
100 w = CSD(2) * ones(1,m_beams.numberElements);
101 hH = CSD(3) * ones(1,m_beams.numberElements);
102 bB = CSD(4) * ones(1,m_beams.numberElements);
103 mainCS=linspace(0,1,sp-2);
104 knots=[0 0 0 0 0 1 1 1 1 1];
105 Nurbs = nrbmak([mainCS(1,:);dims(4,:)],knots);
106 Oi = nrbeval(Nurbs,linspace(0,1,(nbeam)));
107
108 O=zeros(1,2*nbeam-1);
109 O(1,1:nbeam)=Oi(2,:);
110 O(1,nbeam+1:2*nbeam-1)=flip(180-Oi(2,1:nbeam-1));
111 O(1,nbeam)=180;
112
113 % rectangle
114 m_beams.H=H;
115 m_beams.w=w;
116 m_beams.height=H; %H+h;
117 m_beams.width=w; %B;
118 m_beams.CStype     = 'rectangle'; %'Hbeam';
119 m_beams.A          = w.*H; %2*B.*h+H.*b;
120 m_beams.Iyy        = H.*w.^3/12; %(H.*b.^3)/12 + 2*(h.*B.^3)/12;
121 m_beams.Izz        = w.*H.^3/12; %(b.*H.^3)/12 + 2*(B.*h.^3)/12 +2*h.*B.*((
    H+h).^2)/4;
122 m_beams.J          = (w.*H/12) .* (w.^2+H.^2);%(2.*B.*h.^3+H.*b.^3)/3; %
    This J is St. Venant torsional constant
123
124 p=[m_beams.X(:,1),m_beams.X(:,2),m_beams.X(:,3)]';
125
126 for nr=1:2*nbeam-1
127     GC(1,nr)=.01*cos(O(1,nr)*pi/180);
128     GC(2,nr)=.01*sin(O(1,nr)*pi/180);
129     GC(3,nr)=0;
130 end
131
132 %%Use this to specify an orientation curve
133 m_beams.GuideCurve = p+GC;
134 m_beams.guidecurve = reshape(m_beams.GuideCurve,3*m_beams.numberNodes,1);
135 plot3(m_beams.GuideCurve(1,:),m_beams.GuideCurve(2,:),m_beams.GuideCurve
    (3,:),'r-');
136 hold on
137
138 for e = 1:m_beams.numberElements-1
139
140 %modified rotRo1 met richting e03 naar bepaald punt (niet de snelste
    versie)
141 x21=(m_beams.X(e+1,1:3)'-m_beams.X(e,1:3)');
142 e01     = (x21)/norm(x21);
143 e03star = cross(e01, m_beams.guidecurve(3*(e-1)+[1:3]) - m_beams.X(e,1:3)
    ');
144 e03     = e03star/norm(e03star);
145 e02     = cross(e03,e01);
146 Ro      = [e01 e02 e03];        % voor eqn 4.28
147
```

```
148 m_beams.tr1(:,:,e)          = eye(3)*Ro;
149 m_beams.tr2(:,:,e)          = eye(3)*Ro;
150
151 end
152 m_beams.tr1(:,:,m_beams.numberElements) = eye(3)*Ro;
153 m_beams.tr2(:,:,m_beams.numberElements) = eye(3)*Ro;
154
155 m_beams.Rg1                 = repmat(eye(3),1,1,m_beams.numberElements);
156 m_beams.Rg2                 = repmat(eye(3),1,1,m_beams.numberElements);
157
158 m_beams.D                   = zeros(6,m_beams.numberNodes)';
159 m_beams.d                   = zeros(m_beams.eqn,1);
160
161 %% BOUNDARY CONDITIONS on begin- and endpoint
162 ep1    = [0 0 0];       ep2    = [0 0 0];
163 theta1 = [0 0 0];       theta2 = [0 0 0];
164
165 Fe  = zeros(m_beams.eqn,1);
166
167 Fmax1=325;
168
169  Fe(nbeam*6-5)=-0.3*Fmax1;  %X
170 % Fe(nbeam*6-4)=-Fmax1; %Y
171 Fe(nbeam*6-3)=0; %Z
172 Fe(nbeam*6-2)=0; %MX
173 Fe(nbeam*6-1)=0; %MY
174 % Fe(nbeam*6-0)=Fmax1*0.2; %MZ
175
176 m_beams.bc  = [1:6  m_beams.eqn-5:m_beams.eqn];
177 bc          = [1:6  m_beams.eqn-5:m_beams.eqn];
178 dofs.dp     = [ep1 theta1 ep2 theta2]';
179 dofs.all    = (1:m_beams.eqn)';
180 dofs.bc     = bc(~isnan([dofs.dp]));
181 dofs.dp     = dofs.dp(~isnan([dofs.dp]));
182 dofs.R      = sparse(1:length(dofs.bc),[dofs.bc],1+0*dofs.bc,length(dofs.
        bc),m_beams.eqn);
183
184 PlotBeamsCrossSections(m_beams,par, 'undeformed')
185 [history, m_beams] = solveNONLINstaticCOR(m_beams,dofs,par,Fe);
186
187 for di=1:nbeam-1
188     diCS(1,1)=m_beams.D(1,2);
189     diCS(1,di+1) =abs((((m_beams.X(di+1,1)-m_beams.X(di,1))^2)+((m_beams.X
            (di+1,2)-m_beams.X(di,2))^2)+((m_beams.X(di+1,2)-m_beams.X(di,2))
            ^2))-(((m_beams.D(di+1,1)+m_beams.X(di+1,1))-(m_beams.X(di,1)+
            m_beams.D(di,1)))^2+((m_beams.D(di+1,2)+m_beams.X(di+1,2))-(m_beams
            .X(di,2)+m_beams.D(di,2)))^2+((m_beams.D(di+1,3)+m_beams.X(di+1,3))
            -(m_beams.X(di,3)+m_beams.D(di,3)))^2));
190 end
191
192
193 disp =[m_beams.D(nbeam,1);m_beams.D(nbeam,2);m_beams.D(nbeam,3)]
194 Ratio = disp(1)/disp(2)
195
196 angleX=zeros(par.nTimestep,1);
197 angleY=zeros(par.nTimestep,1);
```

```
198 angleZ=zeros(par.nTimestep,1);
199 for qz=1:par.nTimestep
200     angleX(qz,1)=history(qz).m.D(nbeam,4);
201     angleY(qz,1)=history(qz).m.D(nbeam,5);
202     angleZ(qz,1)=history(qz).m.D(nbeam,6);
203 end
204 angleXX=sum(angleX);
205 angleYY=sum(angleY);
206 angleZZ=sum(angleZ);
207
208 angleZZZ=angleZZ*180/pi
209
210 for k=1:sp-1
211 plot3([X(1,k),X(1,k+1)],[X(2,k),X(2,k+1)],[X(3,k),X(3,k+1)], 'b-.')
212 end
213 plot3(X(1,:),X(2,:),X(3,:),'r*')
214 PlotBeamsCrossSections(m_beams,par, 'undeformed')
215 xlabel('x(m)')
216 ylabel('y(m)')
217 zlabel('z(m)')
218 % isoforceplotsWrist(dims)
219 dragzoom()
220 grid on
```

A.9. ShapeOptmultiWrist MATLAB® code

```
function [error] = ShapeOptmultiWrist(dims)
%%
Fmax=325;
% Fmax=10;
nbeam=20;

% DISTANCES
Fe = zeros((nbeam*2-1)*6,1);
Fe(nbeam*6-5)=-Fmax*1.0;
dis(1,:)=ShapeOptWrist(dims,Fe);
error=abs(0.1+dis(1,1));

Fe = zeros((nbeam*2-1)*6,1);
Fe(nbeam*6-4)=-Fmax*1.0;
dis(2,:)=ShapeOptWrist(dims,Fe);
error=0.01+dis(2,2)+error;

Fe = zeros((nbeam*2-1)*6,1);
Fe(nbeam*6-0)=Fmax*1.0*0.2;
dis(3,:)=ShapeOptWrist(dims,Fe);
error=abs(0.5236-dis(3,6))+error
end
```

A.10. Investigation in characterization methods of Compliant Mechanisms

Investigation in characterization methods of Compliant Mechanisms

Tom Cratsborn, Ali Amoozandeh Nobaveh, Giuseppe Radaelli and Just L. Herder
Department of Precision and Microsystems Engineering
Delft University of Technology

***Abstract*—Compliant Mechanisms are relatively new mechanisms that have many advantages over more traditional rigid-body mechanisms. Their application becomes more common due to increased understanding and improvements in computational hardware and software. To better understand the stiffness and kinematic behaviour of complaint mechanisms, modelling, characterzation and synthesis methods were developed. In this paper, the different methods, which are Potential Energy, Force, Stiffness Fields, Freedom and Constraint Topologies (FACT) and building block approaches e.g. Compliance and Stiffness Ellipsoids, Eigentwist/Eigenwrech and Instant Center are evaluated. The goal of this paper is to (1) explain the differences between these methods with the latest gathered developments and specify their advantages and disadvantages. (2) Help the reader determine which method is most suited for particular shapes, deflection paths, strategies of the designer or insightful visualization.**

***Index Terms*—compliant mechanisms, characterization method, Freedom and Constraint Topologies, Compliance and Stiffness Ellipsoids, Eigentwist and Eigenwrench, Potential Energy Fields, Instant Center**

I. Introduction

Complaint Mechanisms are flexible mechanisms that transfer an input force or displacement to another point through elastic body deformation. [1] They are relatively new compared to traditional rigid-body mechanisms that consist of rigid links connected at movable joints. In Figure 1, a compliant forceps is shown where the movable joints are replaced by compliant hinges. Replacing rigid-body mechanisms with compliant mechanisms has many advantages and more people are beginning to understand them [1], [2].

Fig. 1. Compliant Forceps [1]

A. Advantages of Compliant Mechanisms

The first advantage of compliant mechanisms is increased performance. This is due to fewer parts, lower weight, no lubrication at joints and low friction, which is beneficial in hostile environments such as vacuum, underwater or in the human body. The second advantage is precise motion. This is due to reduction or elimination of backlash and wear. The third advantage is lower cost due to fewer parts, reduced manufacturing time, reduced assembly time and simplified manufacturing due to the various possible production processes (e.g. stamping, machining, 3D printing, injection moulding, laser and a water-jet cutting.) The fourth advantage is the ability to miniaturise due to simplified fabrication.

B. Challenges of Compliant Mechanisms

However, compliant mechanisms also give challenges. The first challenge is that compliant mechanism analysis and design is typically more difficult than for rigid-body mechanisms because forces and movements are always coupled due to elasticity. This requires the simultaneous design for force and motion behaviour. The second challenge is that fatigue life needs to be addressed. This is because repeated stress at bending locations can lead to a shorter fatigue life than the desired lifetime of the mechanism. The third challenge is that consumer perception needs to be addressed because flexible components could be perceived as weak and flimsy. The fourth challenge is motion is often more limited compared to traditional rigid-body mechanisms, limited by the deflection it can undergo before failure. The fifth challenge arises when a compliant mechanism is under conditions such as being held under stress for long periods or elevated temperatures, i.e. creep. This could lead to a new shape with possibly undesired behaviour. The sixth challenge appears when a compliant element integrates both a spring and hinge function. This allows possibly undesired behaviours.

Compliant mechanisms are becoming more common due to improvements in our understanding of compliant mechanisms, together with technological developments. Examples of technological developments are new materials that are well suited for compliant mechanisms, improvements in computational hardware and software to analyse motion and stresses. Also considerable effort has gone into creating methods that increase our ability to develop compliant mechanisms. Moreover, the developments in manufacturing,

especially 3D printing, have lead to rapid prototyping to help better understand compliant mechanism behaviour.

C. Development Process of Compliant Mechanisms

There are three phases in the development process of compliant mechanisms: Modelling, Characterization and Synthesis.
Modelling is the first phase, this is an analysis of the behaviour and performance of compliant elements and mechanisms. The goal is to obtain the model for a given mechanism to choose acceptable values for design parameters (such as thickness and length) or verify the performance of this design.
Characterization is the second phase. For a given mechanism, the deflection behaviour is characterized by the model obtained from the analysis in Modelling. Characterization methods give information about the kinematic behaviour and stiffness of compliant mechanisms.
Synthesis is the third and final step, using the model from the analysis to come up with new mechanisms with new behaviours. Mechanisms can also be synthesised with information obtained by characterization methods, using this information to synthesize the design for a more desirable behaviour.

This paper is conducted to help successfully develop compliant mechanisms by understanding different characterization methods better and for which characterization goal, which method is most suitable. The objective of this paper is to explain the differences between the characterization methods and determine which method is most suitable for which application based on increased understanding and gathering of the latest research. The gathering and comparison of characterization methods has not been done before in any paper. However, comparable studies have been done on the complete development process of compliant mechanisms by Howell et al. [2] and an overview of synthesis methods by Gallego Sanchez and Herder [3].

This paper is organised as following. In chapter II, the five characterization methods are explained. In chapter III, the methods and their advantages and disadvantages are compared. In chapter IV, the differences between the characterization methods are discussed and set of goals is given for which applications, which method is best to apply. Then in chapter V, the paper is concluded.

II. Characterization Methods

This literature report is focused on the characterization methods of compliant mechanisms, to find what is and is not currently possible with these methods. Their fundamental working principles are explained and each method is extended with the latest developments. The characterization methods are Freedom and Constraint Topologies, Compliance and Stiffness Ellipsoids, Eigentwist/Eigenwrench, Instant Center Approach and Potential Energy Fields. The methods will be elaborated in the next sections.

A. Freedom and Constraint Topologies (FACT)

FACT is a comprehensive library of geometric shapes that represents the mathematics of screw theory [2]. The FACT method enables designers to visualise the regions wherein all compliant constraint elements could be placed that would allow the mechanisms desired degrees of freedom. The library contains all the relevant quantitative information that is needed to quickly generate complex concepts based on kinematic, elastomechanic and dynamic design requirements without many difficulties that appear when one focuses on detailed mathematical treatments. This method is extensively described below due to the many advancements in the method. Also, the method is somewhat abstract [4]; therefore "a more detailed explanation is required before the utility becomes apparent."
The FACT library contains two sets of complementary geometric shapes. One set is called freedom spaces which shows the motions that are permitted or the DOFs of a flexure system. The other set is called constraint spaces, which shows the area's where the compliant constraints could be placed that would allow those DOFs. Flexure systems synthesised are best suited for precision applications, when deflections are at least three orders of magnitude smaller than the mechanism's size. This subsection does not explain how FACT could be used to design flexure systems that guide a stage along a desired motion path but on systems that have desired DOFs or degrees of compliance (DOCs). This subsection also focuses on kinematic flexure synthesis only so not on considerations of stiffness and dynamics.
There are different types of flexure systems: (1) Parallel flexure systems have a single stage that is directly connected to the ground by non-conjugated compliant elements [5]. (2) Serial flexure systems consist of parallel modules that are stacked together as a successive chain. (3) Hybrid flexure systems consist of a mix of parallel and serial flexure systems. Hybrid flexure systems are analysed in Hopkins [6]. These different types of flexure systems are visualized in Figure 2. This first part of this subsection is focused on parallel flexure systems, not serial and hybrid flexure systems. However, subsection II-A6 extends about serial flexure systems.

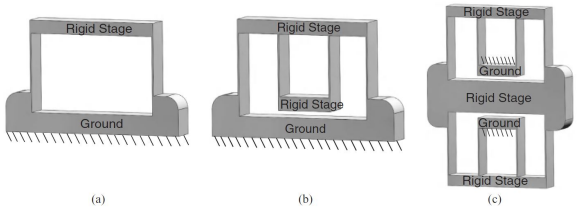

Fig. 2. Parallel (a), serial (b) and hybrid (c) flexure systems [5].

1) Fundamental Principles: This subsection explains the underlying principles needed to understand the FACT approach. Motions and constraints are modelled using screw

theory and shown using geometric entities. Principles of kinematic equivalence are presented to generate alternative design concepts with the exact same DOFs.

2) Modelling motions using Screw Theory: In screw theory [7], [8], any extremely small motion is a screw motion that may be modelled as a 6x1 vector that is a twist, **T**. This can be described by a line that is simultaneously the axis of rotation and the line along which translation of a body occurs. The rate to which the stage translates to which it rotates is the pitch of a screw motion. For a pitch of zero, the motion is a rotation. For an infinite pitch, the motion is a translation. For any other pitch value, the motion is a screw. Illustrations of these three motion types are shown in Figure 3.

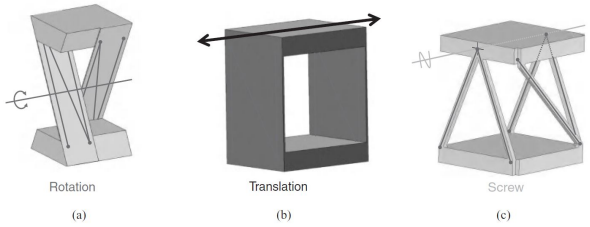

Fig. 3. Parallel flexure systems that have a rotational DOF (a), a translational DOF (b) and a screw DOF (c) [2].

3) Modelling constraints using Screw Theory: Compliant constraints are only able to transmit combinations of forces on stages that are constrained by them. They can be described by sets of lines which are collinear with the axes of forces that the constraints are able to impart. In screw theory, each of these constraint lines can be modelled by a pure force 6×1 vector called a wrench, **W**. When the compliant constraint is long and slender like a wire flexure, shown in Figure 3c, a single wrench directed along the axis of constraint accurately models the constraint. When the compliant constraint is a blade/leaf flexure, shown in Figure 3a and 3b. The constraint lines set that connects the stage to the ground and lies on the plane of the blade, precisely models the compliant constraint. Example sets of constraint lines are shown in Figures 3a and b on each flexure.

The relationship between a compliant mechanism DOFs and DOCs is demonstrated by the rule of complementary topologies [9]. This rule explains that each freedom space uniquely relates to a complementary constraint space. The constraint space is the geometric structure that shows the area wherein compliant constraints are placed for allowing the DOFs that are desired within the freedom space. From a design stand point, the concept of constraint space is highly effective. If one knows which constraint space uniquely links to the freedom space, one is able to quickly visualize all concepts within the constraint space that satisfies the desired kinematics.

In Maxwell [10], a basic mathematical relationship is formulated that explains for a constraint mechanism to only have the wanted n DOFs shown by its freedom space. 6–n independent constraint lines have to be chosen from the complementary constraint space. For determining the amount of independent constraint lines from a specific group, Gaussian elimination can be used to the wrench vectors that model them. A substitute to Gaussian elimination is a comprehensive list of qualitative "rules of thumb" that can guide a designer to select independent constraint lines from any constraint space. Once the desired number of independent constraint lines is chosen from a constraint space, other selected constraint lines from the equivalent space are redundant thus do not change the mechanism's kinematics. Despite the fact that redundant constraints do not change the mechanism's DOFs, they do however change the mechanism's load capacity, stiffness, symmetry and dynamics. Constraint space is not only useful for aiding designers to synthesize constraint mechanisms to attain the wanted DOFs set. Yet it is also important for aiding designers to visualizing area's where each redundant constraint is located for optimizing other design parameters without changing the kinematics of the mechanism.

4) Comprehensive Library of Freedom and Constraint Spaces: This approach is comprehensive because there are a limited amount of complementary freedom and constraint space pairs. These pairs are visualized in Figure 4 and further described in detail in [11], [12]. In this subsection, the reader does not have to understand all information in Figure 4. However, it is relevant to know that all the spaces belong to one of the six columns and each column refers to the amount of DOFs shown by freedom spaces in each column. There is no 6 DOFs column because a system with six DOFs is not constrained.

Every freedom space is shown on the left of the double sided arrow and every complementary constraint space is shown to the right of this arrow. Furthermore, note that the 1 DOF column has only three types of freedom and constraint space pairs. This is due to the fact that in screw theory only three types of motions exist: translations, rotations and screws. Also notice that the library of spaces shown in Figure 4 is only comprehensive for parallel flexure systems. Other freedom spaces are not shown in Figure 4 that are achievable by serial flexure systems. These are shown later in subsection II-A6.

5) Kinematic Equivalence: Compliant constraint elements that have the same kinematic but different geometric, dynamic and elastomechanic characteristics are named kinematically equivalent. Such compliant constraint elements can be interchanged without changing the flexure mechanism's DOFs. This allows one to examine multiple concepts that have the same wanted kinematic design requirements.

6) Serial Flexure Systems: The previous part was focused on parallel flexure systems. However, a lot of research has also been done on serial flexure systems. Synthesizing serial flexure systems is often more difficult than parallel flexure systems [5]. For synthesis of a parallel flexure system, it is hard to keep track of (1) the relative three dimensional orientations of the flexure constraints, (2) the orientation of the allowed motions and (3) the three dimensional relationships between

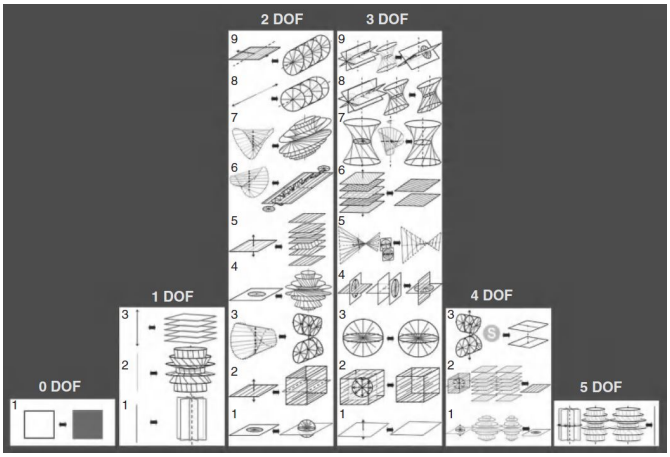

Fig. 4. FACT library of freedom and constraint spaces for parallel flexure systems. Every column relates to the amount of DOFs the type's freedom space has. In every column, the freedom and constraint pairs are defined with type numbers. Each type's freedom space is shown to the left of the double-sided arrow and to the right of this arrow the constraint space of the same type is shown [2].

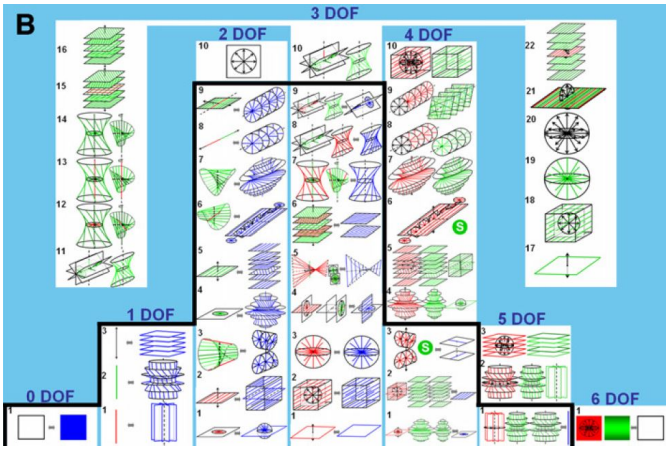

Fig. 5. Practical FACT chart for synthesis. Every column relates to the amount of DOFs the type's freedom space has. In every column, the freedom and constraint pairs are defined with type numbers. Each type's freedom space is shown to the left of the double-sided arrow and to the right of this arrow the constraint space of the same type is shown [5].

each constraint and the allowable motions. For synthesizing a serial flexure system, the previous becomes even harder as extra stages are stacked on each other. It is harder because the kinematics, dynamics and elastomechanics of one stage are influenced by the kinematics, dynamics and elastomechanics of another stage. The capability to synthesize serial flexure systems is essential because serial flexure systems have advantages over parallel flexure systems like:

- Serial flexure systems can have DOFs that parallel flexure systems do not have.
- Serial flexure systems can be synthesized to have larger ranges of motion than same size parallel systems.
- Serial flexure systems can be synthesized to decrease parasitic errors.

The FACT library for serial flexure systems is shown in Figure 5. Interestingly, there are only fifty freedom and constraint space pairs called types.

Building Blocks

In the next subsections three models to characterize the primary functional behaviour of a building block are elaborated. These models are part of the building block approach and were developed by Kim and Krishnan in [13]–[15]. Therefore, the explanation of this approach and the models are grouped together. An important disclaimer to note is that also fields and the FACT method can be used as building blocks to describe the kinematic behaviour of a subsystem. However, this section provides input for the next three sections and are therefore also grouped together. The building block approach is intuitive and provides key insight into how individual building blocks contribute to the overall behaviour of a system. The basis of this approach is that a mechanism can be decomposed into a number of submechanisms or building blocks. If a single building block cannot perform a desired kinematic task, the task is decomposed in subtasks. These subtasks are tested against a library of available building blocks until a suitable building block is found. Decomposition is a nontrivial task which needs familiarity with overall system behaviour and building blocks that meet the requirements of the subproblem. When one becomes more familiar with the capabilities of a building block set, one can better integrate the blocks into the overall system.

The elements that are required for building block mechanism characterization are: a library of building blocks and models to characterize the primary functional behaviour of a building block.

Library of Fundamental Building Blocks: Two fundamental building blocks, the compliant dyad and 4-bar are introduced. These two simple building blocks can address a wide range of design problems when they are combined in parallel or series.

The Compliant Dyad (CDB), shown in Figure 6(a), consists of two beams that are connected in series. The beams have different lengths l_1 and l_2 and have different orientations, given by α. The second beam length is normalized so that $l_{2norm} = l_2/l_1$.

The Compliant 4-bar (C4B), shown in Figure 6(b), consists of a CDB and a cantilevered beam. The C4B has an input and output which are constrained to displace along specific directions.

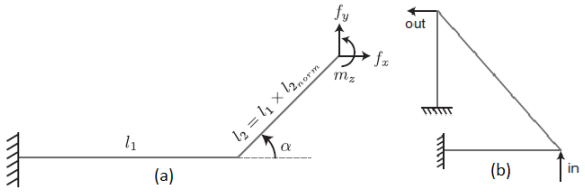

Fig. 6. (a) Compliant Dyad and (b) Compliant 4-bar [5]

Elastokinematic Representations to Model Functional Behaviour: The kinematic behaviour of a compliant mechanism is strongly coupled to the loads that are applied to it. This coupling is captured in the stiffness matrix and its inverse the compliance matrix. The stiffness in a point (e.g. endpoint, end-effector, etc.) in 2D is a 3x3 matrix and in 3D a 6x6 matrix. The size of a global stiffness matrix, of e.g. a finite element model, for a system depends on the amount of nodes and can be thousands of times larger than the matrix in a point.

Otherwise the reader may think that it is the global stiffness matrix of, e.g., a finite element model. These matrices, depending on the amount of nodes, could be thousands of times larger.

$$\mathbf{F} = [K]\mathbf{U}; \quad \mathbf{U} = [C]\mathbf{F}; \quad [K] = [C]^{-}1 \tag{1}$$

where **U** = Generalized displacement vector; **F** = Generalized load vector; [K] = Stiffness matrix; [C] = Compliance matrix;

The generalized displacement vector (**U**) captures both translations and rotations. The generalized load vector (**F**) captures both forces and moments. Unfortunately, both stiffness and compliance matrix do not highlight functional behaviour in and of themselves. Also matrix decomposition methods do not yield meaningful information either. Therefore, Compliance Ellipsoids, Eigentwist/-wrench and Instant Centers are introduced because these geometric representations capture that fundamental mechanism behaviour.

B. Compliance and Stiffness Ellipsoids

The compliance ellipsoid is a concept to represent the magnitude and direction of compliance forces at a collision point. Asada [16] defined the generalized inertia ellipsoid to represent the inertia properties and dynamic behavior of a manipulator. Also, Yokoi [17] derived the joint compliance and stiffness matrix in developing a compliance control algorithm for manipulators. Compliance ellipsoids generated have been used in robotics to identify possible locations of an end effector under external load when its actuators are fixed [18]. Kim [15] shows that compliance ellipsoids capture the kinematic behaviour because they transform the generalized force vector $F = \begin{bmatrix} f_x & f_y & m_z \end{bmatrix}$ to the generalized displacement vector $U = \begin{bmatrix} u_x & u_y & \theta \end{bmatrix}$. Vecotr F can be described as $\begin{bmatrix} F & F & FL \end{bmatrix}$ and U as $\begin{bmatrix} L & L & 0 \end{bmatrix}$. The compliance matrix transforms **F** to an completely different sort of vector. To address this discrepancy, a normalizing length, l, is introduced to relate m_z to f_x and f_y and θ to u_x and u_y. This normalizing length depends on the size of the geometry and is defined as an example for a compliant dyad building block in the previous section. This reformulations leads to:

$$U = \begin{bmatrix} u_x u_y \theta \end{bmatrix} = \begin{bmatrix} u_x u_y u_\theta / l \end{bmatrix} \tag{2}$$

$$F = \begin{bmatrix} f_x f_y m_z \end{bmatrix} = \begin{bmatrix} f_x f_y l f_m \end{bmatrix} \tag{3}$$

Typically, l assumes a nominal length of the building block's scale. When we reformulate the force-displacement relationship with respect to l. The following can be obtained:

$$U = \begin{Bmatrix} u_x \\ u_y \\ u_\theta / l \end{Bmatrix} = CF = C \begin{Bmatrix} f_x \\ f_y \\ l f_m \end{Bmatrix} \tag{4}$$

$$\begin{pmatrix} 1 & 0 & 0 \\ 0 & 1 & 0 \\ 0 & 0 & \frac{1}{l} \end{pmatrix} \begin{Bmatrix} u_x \\ u_y \\ u_\theta \end{Bmatrix} = C \begin{pmatrix} 1 & 0 & 0 \\ 0 & 1 & 0 \\ 0 & 0 & l \end{pmatrix} \begin{Bmatrix} f_x \\ f_y \\ f_m \end{Bmatrix} \tag{5}$$

$$\implies \tilde{U} = \begin{Bmatrix} u_x \\ u_y \\ u_\theta \end{Bmatrix} = \begin{pmatrix} 1 & 0 & 0 \\ 0 & 1 & 0 \\ 0 & 0 & l \end{pmatrix} C \begin{pmatrix} 1 & 0 & 0 \\ 0 & 1 & 0 \\ 0 & 0 & l \end{pmatrix} \begin{Bmatrix} f_x \\ f_y \\ f_m \end{Bmatrix} = \tilde{C}\tilde{F} \tag{6}$$

The normalized compliance matrix, $\tilde{C}$ transforms $[\tilde{F}] = [F, F, F]$ to $[\tilde{U}] = [L, L, L]$. This transformation can be decomposed using traditional matrix methods due to the fact that the units are consistent. $\tilde{C}$ transforms a unit force sphere to a compliance ellipsoid and this is shown in Figure 7. The semi-axes of the ellipsoid are the eigenvalues and eigenvectors of $\tilde{C}$. We classify the primary compliance vector (PCV), secondary compliance vector (SCV) and tertiary compliance vector (TCV) as shown in Figure 7. The PCV is the most flexible direction and the TCV is the most stiff direction.

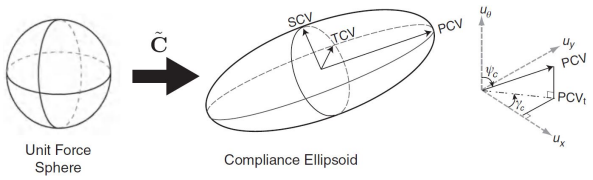

Fig. 7. The normalized compliance matrix $\tilde{C}$ transforms the unit force sphere (left of the arrow) to the compliance ellipsoid (right of the arrow). The direction of the PCV can be described by angles ψ and γ [2].

The most important characteristics that compliance ellipsoids describe are:

- γ : The angle between u_x and the projection of PCV onto the u_x u_y - axis.
- ψ: The angle between the u_θ -axis and the PCV. ψ measures the coupling between rotational translation components in the PCV. As $\psi \to 0°$, the PCV becomes purely rotational. Vice versa, as ψ goes to 90° the PCV becomes a pure translation.
- n_2: The absolute ratio of the SCV over the PCV. This expresses how much stiffer the SCV is compared to PCV.

A drawback of ellipsoids is that they can be misleading. Their shape suggests that it gives stiffness information in each direction but it solely does this in the principal directions because those are the only directions where displacement and force are exactly in the same direction. This means that it does noes give stiffness information along all directions, except for their semi-axis directions, but their shape suggests so. Another drawback of ellipsoids is that two are needed, one for translation and one for rotation, to describe the kinematic behaviour

of a specified point. This makes it difficult to plot ellipsoids for large deflections. An example of a mechanism with the translational compliance ellipsoids and rotational compliance ellipsoid is show in figure 8. It also means that ellipsoids do not show the coupling between rotations and translations which is important to describe kinematic behaviour.

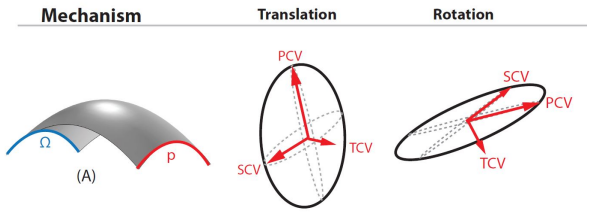

Fig. 8. Shell mechanism with relative degrees of freedom with a blue constraint line and red actuation line. The symmetric point on the red actuation line was used to determine the compliance matrix from [19].

C. Eigentwist and Eigenwrench

In the previous subsection compliance ellipsoids were explained. However, using an arbitrary normalizing length compromises the representation's mathematical robustness. Therefore, the eigentwist and eigenwrench characterization can be a more suitable representation.

This method is based on screw theory which was first used by Ball [20]. Eigenscrews to characterize system properties have been examined by Griffis and Duffy [21]. The first time they are used to classify compliant systems was examid by Patterson and Lipkin [22].

The eigentwist/eigenwrench method decouples translational and rotational terms from the compliance matrix without introducing a normalizing length. This is possible in 2D at the center of elasticity (CoE). The resulting characterization is intrinsic to the geometry and leads to insightful functional characterization.

This method consists of eigentwists and eigenwrenches that generalize the concept of a center of compliance [23]. The Eigentwist is a twist on the axis that produces a parallel couple. The Eigenwrench is a wrench on the axis that produces a parallel translation. There are two problems with using eigenscrews for a decomposition. First, the diagonalized elements have a limited physical meaning. Second, a complete set of eigenscrews does not always exist for the singular cases.

1) Decoupling translations and rotations: The eigentwist and eigenwrench decomposition can be defined by two generalized eigenvalue problems

$$C\mathbf{F} = a_f \tilde{\eta}\mathbf{F}; \quad K\mathbf{U} = k_g \tilde{\xi}\mathbf{U} \tag{7}$$

where C and K are the compliance and stiffness matrices, and **U** and **F** are the generalized displacement and force vectors. $\tilde{\eta}$ and $\tilde{\xi}$ normalize the translational and rotational parameters of the compliance and stiffness matrix. Shown by the following

$$\tilde{\eta} = \begin{bmatrix} I & 0 \\ 0 & 0 \end{bmatrix}; \tilde{\xi} = \begin{bmatrix} 0 & 0 \\ 0 & 1 \end{bmatrix} \tag{8}$$

where I is the identity matrix. a_f only contains values for translational compliance while k_g only contains rotational compliance parameters.

2) Description of the Eigentwist and Eigenwrench parameters: The decomposition shown is effective in decoupling translational and rotational parameters in the compliance matrix but the associated terms have to be mapped to the mechanism geometry to get insightful characterization. The terms are the following:

- Center of Elasticity (CoE): One of the most important characteristics of planar geometries is the center of elasticity. This is a unique point where translations and rotations are decoupled. At the CoE, any force that is applied leads to a pure translation and any moment applied leads to a pure rotation, if we assume a rigid connection with the input.
- Translational Compliance: At the CoE, there exist two jointly perpendicular directions where any force applied leads to a pure coincident translation.
- Eigenrotational Stiffness (k_g): The eigenrotation stiffness is the ratio of the flexural rigidity to the overall length and gives the reaction moment generated by a pure unit rotation at the CoE.

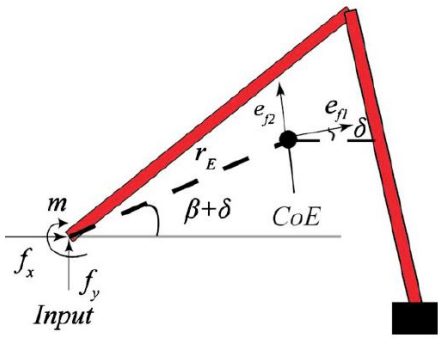

Fig. 9. Eigentwist and eigenwrench parameters for a particular building block geometry [13].

Each of the above eigentwist and eigenwrench terms can be obtained from the parameters of the stiffness matrix. The compliance can be shown by the eigentwist and eigenwrench characterization using geometrically applicable parameters. However, these parameters by themselves may not help for insightful decomposition of a problem. To enable this, a graphical representation of the parameters is shown in Figure 9.

3) Extension to large deflections: In [24], a method is introduced for the characterization of non-linear behaviour for large deflections in compliant mechanisms. This method

considers coupling and allows the comparison of stiffness between all six DOFs and the results are shown in Figure 10. The characterization is based on consistently derived non-arbitrary unification variables based on equivalent compliance by virtual load and potential energy and therefore it allows the comparison of compliance between DOFs of different mechanisms. With this introduced comprehensive comparison the opportunity rises to order all DOFs, within and between mechanisms in terms of compliance. The most dominant DOFs can now be identified along the trajectory of large deflections of compliant mechanisms. The characterization can be done for any mechanism which has a symmetric positive definite compliance matrix. This results in all real positive eigenvalues which is expected for a compliance matrix.

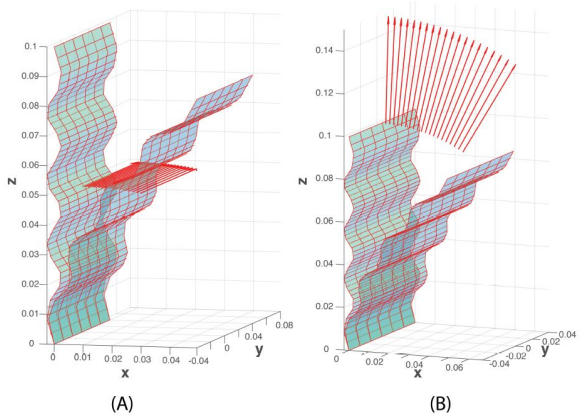

Fig. 10. Large deflections shown for two eigentwist vectors [19].

D. Instant Center Approach

The instant center (IC) has been used for many years in rigid body mechanisms, typically for the analysis of the mechanism [25]. One of the most well know examples where the instant center is used, is the design of an optical galvanometer [26]. To determine the IC, the Aronhold-Kennedy theorem can be used which uses the geometric information of the linkage structure [27]. Klein [28] proposed another way to determine the IC which is a graphical trial and error method based on geometrical and numerical information. The instant center approach gives insight in the kinematic behaviour of a mechanism. The instant center is the point fixed to a body undergoing planar movement that has zero velocity at a particular instant in time. At this instant, the velocity vectors of the trajectories of other points in the body generate a circular field around this point. Therefore, the instant center must lie perpendicular to each PCV (defined in III-B). The instant center is often used for the velocity analysis of planar mechanisms, i.e. (modifications of) compliant four-bar and dyad building blocks.

For a single-input-single-output (SISO) geometric advantage problem, it gives insight in the ratio between magnitudes of displacement at the input and output port in the desired directions of displacement. For the SISO geometric advantage problem, there are three specifications important: The input

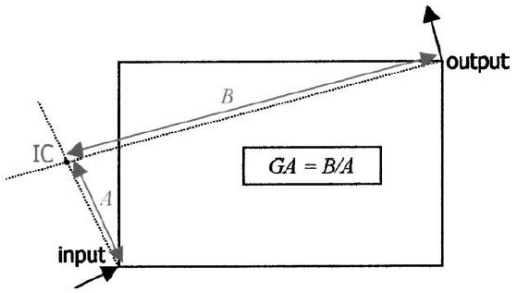

Fig. 11. Geometric advantage presented for a location and PCV of input and output [14].

and output port locations, the PCV at input and output and the desired geometric advantage, as shown in Figure 11. The intersection of the lines perpendicular to each PCV is where the instant center is. The instant center is valid for infinitesimal displacements from the rest position of the mechanism.

Two assumptions must be applicable for using the instant center building block method:

- The floating link behaves approximately as a rigid body.
- The infinitesimal behaviour of the building block can be used to predict the general behaviour throughout the range of motion.

These assumptions can hold or be violated based on the synthesis of a mechanisms. To aid the designer, we investigate the error in geometric advantage. Geometric advantage is defined as the percentage difference of the calculated geometric advantage based on a finite element analysis and the target geometric advantage.

Consider the compliant four bar building block, shown in Figure 12. The coordinates of ground (A), input (B) and output (C) are fixed. Moving junction (D) can be located at any arbitrary point in space and ground (E) is moved along in order to keep the instant center fixed as well.

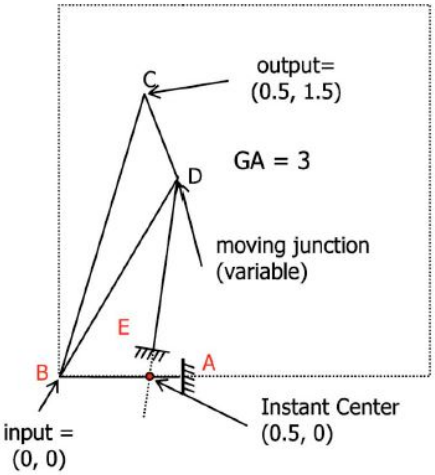

Fig. 12. C4B with coordinates of ground (A)(E), input (B), output (C) and moving junction (D) [14].

In Figure 13, the geometric error based on the location of moving junction (D) is plotted. For all configurations, all beams have the same cross sections. Lengths of AB and DE do not change. As you can see, the geometric advantage is not constant for various locations of the moving junction even though the location of instant center remains the same. Consider the example when the moving junction (D) is located at (2, 0.2) where there is significant error in geometric advantage. Beam AB and DE are nearly in line and for deflections the instant center changes positions. In this configuration, infinitesimal behaviour can not be used to predict the general behaviour of the mechanism. In general, to decrease the error in geometric advantage one could change the length and the thickness of the beams. For this example, obtaining the desired geometric advantage would probably violate space and fabrication limitations.

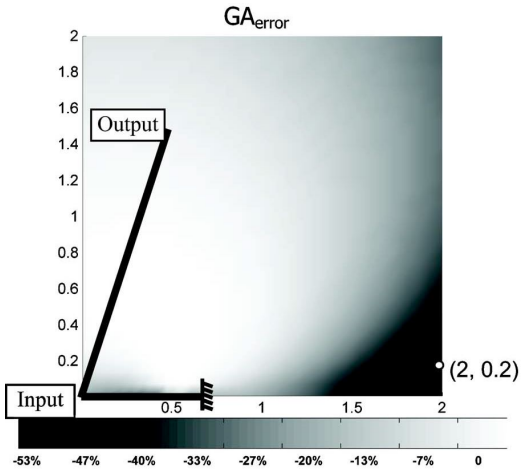

Fig. 13. Geometric error for various locations of moving junction (D) [14].

The generalization of this concept to a three dimensional space is that of a twist around a screw. The screw has an axis which is a line in 3-dimensional space and the screw also has a finite pitch. The instant center method is not applied to size and geometry optimization because the method has a limited role in the design process. This role is limited to mechanism topology generation in the beginning of the design process.

In [29], a new instant center analysis method for planar closed chains is introduced. The previous IC analysis method uses geometrical information from the mechanism configuration. This has the disadvantage of complexity in calculation and difficulty determining the direction of the linkage motion because of geometric complexity. The proposed IC analysis method suggests a new method for planar closed chains. It determines the instant center basically from the relation between joint velocities based on the graphical representation. Twists in screw theory are used to define joint velocities in a closed chain and calculating the IC.

E. Potential Energy/ Force/ Stiffness Fields

The first characterization method is Potential Energy/ Force/ Stiffness Fields. Fields show the behaviour of a chosen point in the shape as when it is deflected. The elastokinematic behaviour of this point can be expressed on the basis of three physical related quantities: energy, force and stiffness, each of these have their own field. Even though the fields are based on related quantities, each field is unique.

In Hogan [30], elliptical isopotential energy contours are used to characterise the endpoint stiffness of a system. Later in English [31], this concept compares the shape of the ellipses to the ispotential lines. Herder [32] uses potential energy graphs of linear extension springs as graphical aid to the synthesis of statically balanced linkages. Extension of the concept when it is applied as a synthesis tool is done by Radaelli [33]. However, only for systems comprising linkages with torsion springs. Radaelli [34], employs potential energy fields for the synthesis of compliant mechanisms. Radaelli [35], shows the application of Potential Energy Fields in three dimensions.

These different fields are explained in more detail below. Obtained from [36], Figures 16, 17 and 18, show the potential energy, force and stiffness fields for deflection of the endpoint for a single rectangular beam (Figure 14) and a double rectangular beam (Figure 15). The double beam is two single beams connected via a pin joint.

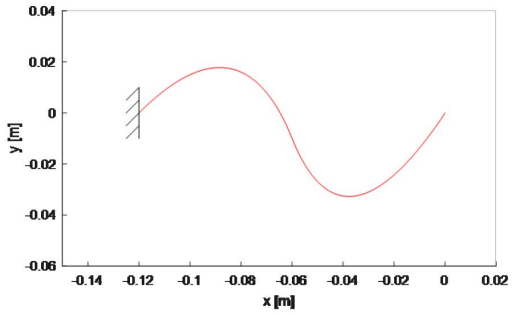

Fig. 14. Single beam which is used for deriving the fields in Figures 16, 17 and 18 [36].

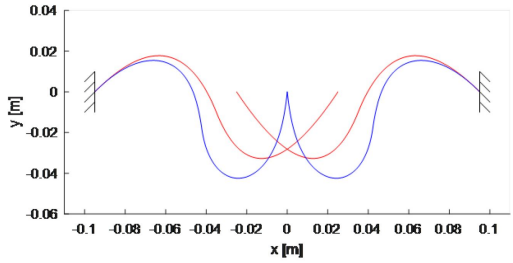

Fig. 15. Double beams. The red beams show the beams when not attached. The blue beams show the beams when attached and prestressed, therefore, also bistable [36]. The latter is used for deriving the fields in Figures 16, 17 and 18.

1) Potential Energy Fields (PEF): Potential energy fields are a collection of known energy points in space [34]. The value of this collection relates to the system's total potential energy when the shape is deformed in space. The energy field is solely produced when all forces are conservative and the

energy is equal to the energy difference of a chosen point that is moved from one position in space to another. At each point, the energy is shown by colour (a), (c) or isopotential (constant energy) lines (b), (d) in Figure 16.

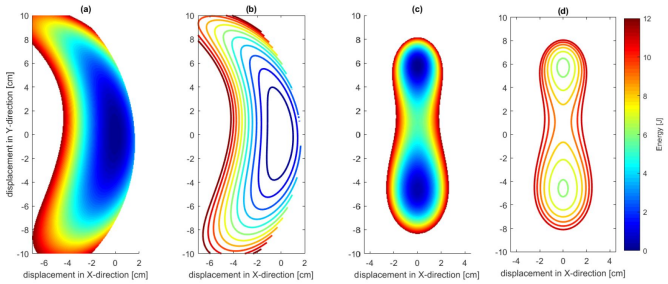

Fig. 16. Energy fields of the single beam (a), (b) and the double beam (c), (d) where the colour shows the magnitude of the force [36].

2) Force Fields: Force fields are a collection of known force points in space. The force may be defined as the force or reaction force necessary to keep the chosen point stationary. The only difference between the two definitions is that the forces are opposite in direction. The fields in Figure 17 show the reaction force of the shape. Another way to visualize force fields is to use isoforce mapping. The isoforce line represents the displacement of a point subjected to a specified force magnitude [36], [37].

3) Stiffness Fields: The stiffness field is a collection of known stiffness points in space. Stiffness shows the change of the reaction force with respect to the deflection. Stiffness is a tensor because it maps the displacement vector to the force vector. At each point in the stiffness field, the tensor correlates to the tangent stiffness of a chosen point when its moved to that point in space. The translational stiffness is a two-by-two tensor in two dimensions and may be decomposed into two principal stiffness components, which are perpendicular and have their own magnitude. Tensor fields are shown by ellipses (a), (c) and Reynolds glyphs (b), (d) in Figure 18.

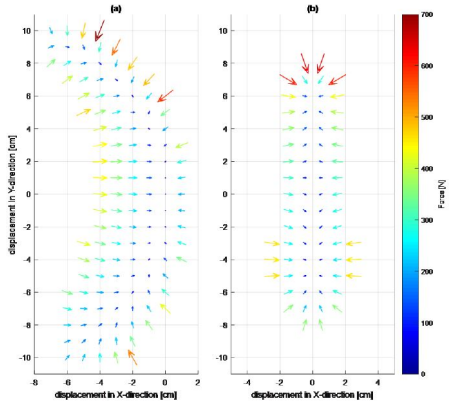

Fig. 17. Force fields of the single beam (a) and the double beam (b). The force is a vector represented by arrows where the length and colour depend on the force's magnitude [36].

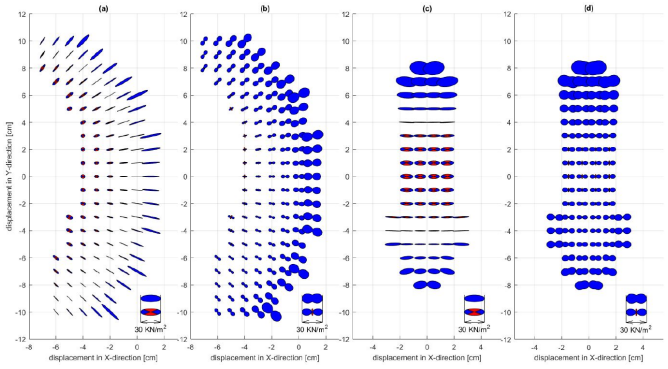

Fig. 18. Stiffness field of single beam (a), (b) and double beam (c), (d). Blue is positive stiffness and red is negative stiffness [36].

These are shapes that can express the value of the tensor in 2D. The radius of the main axis of ellipses and glyphs show the absolute value of principal stiffness. The radius of the Reynolds glyph shows the displacement component parallel to a unit force in that direction and the principal compliances in the principal directions.

III. Results

A. Freedom and Constraint Topologies (FACT)

A comprehensive overview of geometric shapes that enables users to quickly evaluate behaviour for specific shapes. This stiffness behaviour is binary i.e. the freedom or constraint directions. These directions are specified for an instantaneous representation of a specific shape. For more complex mechanisms, the distinction between freedom and constraint directions can become more blurred. FACT is a vizualisation method that enables early-stage flexure system design via "paper and pencil sketches" which means that it requires no computer or FEM analysis to apply. Lastly, the method gives stiffness information for three translations and three rotations. The FACT method has been developed enormously over the years and it has become an extensive library of possible topologies for the design of mechanisms with specified freedom and constraint directions.

B. Compliance and Stiffness Ellipsoids

This method is based on transforming the stiffness and compliance matrix in the force-deflection relationship. It gives good insight into the mechanism's primary kinematic behaviour in three dimensions. However, large deflections and non-linearities are not well dealt with because it is an instantaneous representation. It is possible though, to create ellipses for large deflections as is shown by stiffness fields. Using ellipsoids for large deflections could be investigated to see if this yields useful information about kinematic behaviour. The absolute stiffness values will be calculated with use of a computer. The disadvantage of this approach is that a normalizing length is introduced to resolve units of length and rotation and force and moment [13].

C. Eigentwist/Eigenwrench

The Eigentwist/Eigenwrech approach is also an instantaneous representation and uses computer calculations to determine the absolute stiffness value. It gives stiffness information for three dimensional translations and rotations. This method is, just like the Ellipsoids, based on the compliance matrix. However, this method does not introduce a normalizing length and therefore does not compromise the mathematical robustness. Kinematic behaviour for large deflections can be visualized by plotting multiple twist and wrench axis for multiple deflections [19]. Another approach to identify the most predominant degrees of freedom along the the trajectory of large deflections (non-linear) of complex compliant mechanisms is the unified stiffness characterization [24]. This comprehensive comparison addresses the coupling between rotations and translations by introducing two physically meaningful unification lengths.

D. Instant Center Approach

Instant centers allow designers to present a synthesis problem using kinematic relationships at the conceptual stage. This method is mostly suited for planar mechanisms i.e. compliant dyad, four-bar and slider crank. The method is based on two assumptions: (1) The floating link behaves approximately as a rigid body. (2) The infinitesimal behaviour of the building block can be used to predict the general behaviour. Characterization using instant centers is intended to predict the behaviour of a building block so its role in the design process is limited to the generation of initial mechanism topology.

E. Potential Energy Fields

Fields are particularly appropriate for compliant mechanisms that have large deflections with nonlinear behaviour. This method can give information about energy for deflections in three dimensions. For fields, values are shown at the intersection of gridlines or at isolines. The values for intermediate points can be estimated using interpolation. This method can be applied to give information about multi-stable mechanisms, their equilibrium points and snapping behaviour. It is suitable for complex shapes with complex behaviour and requires finite element analyses.

IV. Discussion

FACT is a hands on method that is particularly suitable for initial "paper and pencil" sketches to rapidly determine freedom and constraint directions. Also for synthesis, a list of suitable topologies to fulfil specific requirements.

The compliance and stiffness ellipsoids give an instantaneous normalized representation of the stiffness behaviour for translation and rotation. Comparing Ellipsoids and FACT as both methods are based on Principal Compliance Vectors (PCVs). For FACT, the freedom and constraint directions can be seen as squeezed ellipsoids.

The ellipsoids and eigentwist/-wrench approach are similar in some sense but the way that the stiffness information is visualized is different. Eigentwist/eigenwrench is more "mathematically robust" because ellipsoids are normalized. Even though the eigentwist/-wrench and ellipsoids are both derived from the stiffness matrix, the way this matrix is transformed and results are derived is completely different.

The instant center approach is particularly suitable for kinematic behaviour of specific planar mechanisms but limited in the design process to the generation of initial mechanism topologies. It is also less suitable for Multiple Input Multiple Output (MIMO) problems. This is because the PCV's are often not perpendicular to the instant center for multiple inputs and outputs.

Potential Energy Fields is the only method that does not use multiple instantaneous representations to explain stiffness behaviour for large deflections but shows this behaviour in a glance. This method also gives insight in snapping behaviour but can take longer due to FEA calculations.

Each characterization method has its pros and cons and it is up to the user to determine which method is most suitable for their specific mechanism.

To aid the user, an overview is given to determine which stiffness characterization method is most suitable:

- If the goal is to quickly get an idea of compliance in multiple directions. FACT is the best method to apply.
- If your goal is to get the kinematic behaviour in three dimension for small deflections. The Ellipsoids or Eigentwist/-wrench are the best methods to apply. Choosing between these two methods should be done on how user wants the results to be visualized. Visualization of kinematic behaviour for large deflections can be done by mapping multiple instantaneous representations.
- For insight in (non-linear) stiffness behaviour of large deflections in a glance, the fields are most suited i.e. Potential Energy, Force or Stiffness fields. For large deflections, choosing between fields and a mapping of multiple Eigentwists/-wrenches also depends on the user's desired visualization. Depending on the application of the user, either method could be more suitable but they can also complement each other.
- If you want to get information about kinematic behaviour for specific planar mechanisms i.e. modifications of compliant dyad, four bar linkage and slider crank, the instant center approach is most suited.

V. Conclusion

This paper explains the basis of five different characterization methods of compliant mechanisms. The method can be based on screw theory, the force-deflection relation or finite element calculations and the applications of each method are provided. The latest developments of each method are added to give the most up to date overview of the possibilities of each method. Furthermore, the pros and cons of the methods are discussed and an overview of different characterization goals or type of mechanisms conclude for which characterization method is most suited. This paper can be extended by focusing on the modelling or synthesis of compliant mechanisms and

define which modelling or synthesis methods are most suited for which design goals with the latest research gathered. Extensions on the FACT method can be researched like large deflection mechanisms with specified motion paths as large deflection compliant mechanisms are used more often and have useful applications. By the same token, extensions to large deflections for ellipsoids can be investigated.

ACKNOWLEDGEMENT

This literature report is part of my thesis of MSc Mechanical Engineering at the Delft University of Technology.

REFERENCES

[1] About Compliant Mechanisms. (n.d.). Retrieved April 20, 2020, from https://www.compliantmechanisms.byu.edu/about-compliant-mechanisms

[2] Howell, L.L., Magleby, S.P., & Olsen, B.M. (2013). eds. Handbook of Compliant Mechanisms. John Wiley & Sons.

[3] Gallego Sanchez, J.A., & Herder, J.L. (2009). Synthesis Methods in Compliant Mechanisms: An Overview. Proceedings of the ASME Design Engineering Technical Conference. 7. 10.1115/DETC2009-86845.

[4] Hopkins, J.B. and Culpepper, M.L. (2006). A Quantitative, Constraint-based Design Method for Multi-axis Flexure Stages for Precision Positioning and Equipment. Proc. of the Annual Meeting of the American Society for Precision Engineering, Monterey, CA, pp. 139–42.

[5] Hopkins, J.B., & Culpepper, M.L. (2011). Synthesis of precision serial flexure systems using freedom and constraint topologies (FACT). https://doi.org/10.1016/j.precisioneng.2011.04.006.

[6] Hopkins, J.B. (2013). Designing hybrid flexure systems and elements using Freedom and Constraint Topologies. Mechanical Sciences. 4. 319-331. 10.5194/ms-4-319-2013.

[7] Ball, R.S. (1900). A Treatise on the Theory of Screws. Cambridge, UK: The University Press.

[8] Phillips, J. (1984). Freedom in Machinery: Volume 1, Introducing Screw Theory. New York, NY: Cambridge University Press.

[9] Hopkins, J.B. and Culpepper, M.L. (2010). Synthesis of multi-degree of freedom, parallel flexure system concepts via freedom and constraint topology (FACT)—Part I: Principles. Precision Engineering, 34: pp. 259–270.

[10] Maxwell, J.C. (1876). General considerations concerning scientific apparatus. Handbook to the Special Loan Collection of Scientific Apparatus, South Kensington Museum London, pp. 1-21.

[11] Hopkins, J.B. (2010). Design of flexure-based motion stages for mechatronic systems via freedom, actuation and constraint topologies (FACT). PhD Thesis. Massachusetts Institute of Technology.

[12] Hopkins, J.B., (2007). Design of parallel flexure systems via freedom and constraint topologies (FACT). Masters Thesis. Massachusetts Institute of Technology.

[13] Krishnan, G., Kim, C.J., & Kota, S. (2010). An intrinsic geometric framework for the building block synthesis of single point compliant mechanisms. Journal of Mechanisms and Robotics, 3(1), [011001]. https://doi.org/10.1115/1.4002513

[14] Kim, C.J., Kota, S.L., & Moon, Y.M. (2006). An Instant Center Approach Toward the Conceptual Design of Compliant Mechanisms, J. Mech. Des. 128 (3) (2006) 542, https://doi.org/10.1115/1.2181992

[15] Kim, C.R., Moon, Y.M., & Kota, S. (2008). A Building Block Approach to the Conceptual Synthesis of Compliant Mechanisms Utilizing Compliance and Stiffness Ellipsoids. https://doi.org/10.1115/1.2821387

[16] Asada, H. (1983). A geometrical representation of manipulator dynamics and its application to arm design. ASME J. Dynamics Systems, Measurement, and Control 105:131–135.

[17] Yokoi, K. (1994). Direct compliance control of robot arm. Ph.D. thesis, Department of Mechanical Engineering Science, Tokyo Institute of Technology.

[18] Lim, H., and Tanie, K. (2000). Human Safety Mechanisms of Human-Friendly Robots: Passive Viscoelastic Trunk and Passively Movable Base. Int. J. Robot. Res., 19, pp. 307–335.

[19] Nijssen, J.P.A., Radaelli, G., Kim, C.J., Herder, J.L. (2016). Overview and kinematic charaterization of compliant shell mechanism building blocks. Mechanism and Machine Theory.

[20] Ball, R.S. (1900) A Treatise on the Theory of Screws. Cambridge at the University Press.

[21] Griffis, M. & Daffy, J. (1990) Kinestatic Control: A Novel Theory for Simultaneously Regulating Force and Displacement. 21st ASME Mechanisms Conference and ASME Journal of Mechanical Design.

[22] Patterson, T. & Lipkin, H. (1990) A Classification of Manipulator Compliance Matrices. 21st ASME Mechanisms Conference, Chicago ASME Journal of Mechanical Design.

[23] Lipkin, H. & Patterson, T. (1992). Geometrical decomposition of robot elasticity. Spatial mechanisms and mechanical system, DE-vol 45, ASME. 10.1007/BFb0031436.

[24] Leemans, J.R., Kim, C.J., van de Sande, W.W.P.J., & Herder, J.L. (December 10, 2018). Unified Stiffness Characterization of Nonlinear Compliant Shell Mechanisms. ASME. J. Mechanisms Robotics. February 2019; 11(1): 011011. https://doi.org/10.1115/1.4041785

[25] Kim, C., Kota, S., & Moon, Y. M. (2006) An instant center approach toward the conceptual design of compliant mechanisms. ASME Journal of Mechanical Design, vol. 128, no. 3, pp. 542-550.

[26] Towfigh, K. (1969) The Four-Bar Linkage as an Adjustment Mechanism. Oklahoma State University Applied Mechanism Conference, Tulsa, OK, pp. 271–274.

[27] Martin, H.G. (2002) Kinematics and Dynamics of Machines. Waveland, Long Glove, IL, USA.

[28] Klein, A.W. (1917) Kinematics of Machinery. McGraw-Hill, New York, USA.

[29] Kim, M., Han, M., Seo, T. (2016). A new instantaneous center analysis methodology for planar closed chains via graphical representation. International Journal of Control, Automation and Systems. 14. 10.1007/s12555-015-0066-3.

[30] Hogan, N. (1985). The mechanics of multi-joint posture and movement control. Biol. Cybern. 52 (5), 315–331, doi: 10.10 07/BF0 0355754.

[31] English, C.E. (1999). Stiffness behaviour in two degree of freedom mechanisms. Ottawa Carleton Institute for Mechanical and Aerospace Engineering, Ottawa, Ph.D. thesis. OCLC: 290494625

[32] Herder, J.L. (2001) Energy-free systems: theory, conception, and design of statically balanced spring mechanisms. PhD Dissertation, University of Technology Delft, Delft, the Netherlands.

[33] Radaelli, G., Gallego, J.A., Herder, J.L. (2010) An energy approach to static balancing of systems with torsion stiffness, in Proceedings of the ASME IDETC/CIE.

[34] Radaelli, G., & Herder, J.L. (2017). A potential energy field (PEF) approach to the design of a compliant self-guiding statically-balanced straight-line mechanism. Mechanism and Machine Theory, 114, 141-155. https://doi.org/10.1016/j.mechmachtheory.2017.04.007

[35] Radaelli, G., Herder, J.L. (2018). Study on the large-displacement behaviour of a spiral spring with variations of cross-section, orthotropy and prestress. Mechanical Sciences. 9. 337-348. 10.5194/ms-9-337-2018.

[36] Doornenbaal, B. (2018). Representing the elasto-kinematic behaviour of compliant mechanisms using fields. MSc Thesis. Delft University of Technology.

[37] Amoozandeh Nobaveh, A., Radaelli, G., & Herder, J.L. Asymmetric Spatial Beams with Symmetric Kinetostatic Behaviour.